



HAL
open science

Large Interferometer For Exoplanets (LIFE)

Óscar Carrión-González, Jens Kammerer, Daniel Angerhausen, Felix Dannert, Antonio García Muñoz, Sascha P Quanz, Olivier Absil, Charles A Beichman, Julien H Girard, Bertrand Mennesson, et al.

► **To cite this version:**

Óscar Carrión-González, Jens Kammerer, Daniel Angerhausen, Felix Dannert, Antonio García Muñoz, et al.. Large Interferometer For Exoplanets (LIFE): X. Detectability of currently known exoplanets and synergies with future IR/O/UV reflected-starlight imaging missions. *Astronomy and Astrophysics* - A&A, 2023, 678, pp.A96. 10.1051/0004-6361/202347027 . hal-04246460

HAL Id: hal-04246460

<https://hal.sorbonne-universite.fr/hal-04246460>






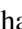
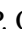

Submitted on 18 Oct 2023

HAL is a multi-disciplinary open access archive for the deposit and dissemination of scientific research documents, whether they are published or not. The documents may come from teaching and research institutions in France or abroad, or from public or private research centers.

L'archive ouverte pluridisciplinaire **HAL**, est destinée au dépôt et à la diffusion de documents scientifiques de niveau recherche, publiés ou non, émanant des établissements d'enseignement et de recherche français ou étrangers, des laboratoires publics ou privés.

Large Interferometer For Exoplanets (LIFE)

X. Detectability of currently known exoplanets and synergies with future IR/O/UV reflected-starlight imaging missions★

Óscar Carrión-González¹, Jens Kammerer², Daniel Angerhausen^{3,4}, Felix Dannert³,
Antonio García Muñoz⁵, Sascha P. Quanz^{3,4}, Olivier Absil⁶, Charles A. Beichman⁷,
Julien H. Girard², Bertrand Mennesson⁸, Michael R. Meyer⁹, Karl R. Stapelfeldt⁸, and The LIFE Collaboration**

¹ LESIA, Observatoire de Paris, Université PSL, CNRS, Sorbonne Université, Université Paris-Cité, 5 place Jules Janssen, 92195 Meudon, France

e-mail: oscar.carrión@obspm.fr; oscar.carrión.gonzalez@gmail.com

² Space Telescope Science Institute (STScI), 3700 San Martin Dr, Baltimore, MD 21218, USA

³ ETH Zurich, Institute for Particle Physics & Astrophysics, Wolfgang-Pauli-Str. 27, 8093 Zurich, Switzerland

⁴ National Center of Competence in Research PlanetS, Gesellschaftsstrasse 6, 3012 Bern, Switzerland

⁵ Université Paris-Saclay, Université Paris-Cité, CEA, CNRS, AIM, 91191, Gif-sur-Yvette, France

⁶ STAR Institute, Université de Liège, Allé du Six-Août 19C, 4000 Liège, Belgium

⁷ NASA Exoplanet Science Institute, Jet Propulsion Laboratory, California Institute of Technology, 1200 East California Blvd, Pasadena, CA 91125, USA

⁸ Jet Propulsion Laboratory, California Institute of Technology, 4800 Oak Grove Drive, Pasadena, CA 91109, USA

⁹ Department of Astronomy, University of Michigan, Ann Arbor, MI 48109, USA

Received 26 May 2023 / Accepted 7 August 2023

ABSTRACT

Context. The next generation of space-based observatories will characterize the atmospheres of low-mass, temperate exoplanets with the direct-imaging technique. This will be a major step forward in our understanding of exoplanet diversity and the prevalence of potentially habitable conditions beyond the Earth.

Aims. We compute a list of currently known exoplanets detectable with the mid-infrared Large Interferometer For Exoplanets (LIFE) in thermal emission. We also compute the list of known exoplanets accessible to a notional design of the future Habitable Worlds Observatory (HWO), observing in reflected starlight.

Methods. With a pre-existing statistical methodology, we processed the NASA Exoplanet Archive and computed orbital realizations for each known exoplanet. We derived their mass, radius, equilibrium temperature, and planet-star angular separation. We used the LIFEsim simulator to compute the integration time (t_{int}) required to detect each planet with LIFE. A planet is considered detectable if a broadband signal-to-noise ratio $S/N = 7$ is achieved over the spectral range 4–18.5 μm in $t_{\text{int}} \leq 100$ h. We tested whether the planet is accessible to HWO in reflected starlight based on its notional inner and outer working angles, and minimum planet-to-star contrast.

Results. LIFE's reference configuration (four 2-m telescopes with 5% throughput and a nulling baseline between 10–100 m) can detect 212 known exoplanets within 20 pc. Of these, 49 are also accessible to HWO in reflected starlight, offering a unique opportunity for synergies in atmospheric characterization. LIFE can also detect 32 known transiting exoplanets. Furthermore, we find 38 LIFE-detectable planets orbiting in the habitable zone, of which 13 have $M_p < 5M_{\oplus}$ and eight have $5M_{\oplus} < M_p < 10M_{\oplus}$.

Conclusions. LIFE already has enough targets to perform ground-breaking analyses of low-mass, habitable-zone exoplanets, a fraction of which will also be accessible to other instruments.

Key words. catalogs – planets and satellites: detection – planets and satellites: fundamental parameters – planets and satellites: terrestrial planets – planets and satellites: gaseous planets – techniques: high angular resolution

1. Introduction

With more than 5000 exoplanets discovered to date, characterizing their atmospheres remains a challenge for most of the cases. Moving from detection to atmospheric characterization is a key step towards understanding the diversity of worlds in our galaxy. This will put our Solar System and the Earth into a broader

context, allowing us to derive statistical conclusions about the prospects for habitability outside our planet. For this, a new generation of space-borne telescopes capable of characterizing potential Earth analogues will be needed.

Transit measurements are so far the main technique available to discover and characterize new exoplanets, with multiple ground-based facilities and space missions such as CoRoT (Baglin et al. 2006), *Kepler* (Borucki et al. 2010), K2 (Howell et al. 2014), TESS (Ricker et al. 2014), and PLATO (Rauer et al. 2014). The population of exoplanets observed in transit is biased towards giant planets on short-period orbits because these create

* Table G.1 is available at the CDS via anonymous ftp to cdsarc.cds.unistra.fr (130.79.128.5) or via <https://cdsarc.cds.unistra.fr/viz-bin/cat/J/A+A/678/A96>

** <http://www.life-space-mission.com/>

stronger signals and are more likely to be observed. The *James Webb Space Telescope* (JWST; Gardner et al. 2006, 2023) will be able to observe and characterize spectroscopically some low-mass exoplanets with lower equilibrium temperatures, mostly orbiting nearby M dwarfs (Beichman et al. 2014; Barstow & Irwin 2016). This will reveal whether small planets around such active stars can retain an atmosphere (Greene et al. 2023) and, if so, will probe their upper atmospheric layers (e.g. Rauer et al. 2011; Wunderlich et al. 2019). Planned for launch in 2029, the Ariel mission (Tinetti et al. 2018) will study the atmospheres of hundreds of warm and hot transiting exoplanets, including some low-mass targets.

Earth analogues orbiting Sun-like stars remain however out of reach for atmospheric characterization with these transit missions. Temperate long-period exoplanets are less likely to be found in transit and, even if found, inherent phenomena such as light refraction will limit the potential for atmospheric characterization (García Muñoz et al. 2012; Misra et al. 2014). Direct-imaging observations are thus needed to analyse the atmospheres of a significant number of temperate low-mass exoplanets.

Several direct-imaging facilities have been proposed for the next decades. On the ground, upcoming extremely large telescopes (ELTs) will be equipped with direct-imaging instruments. The first generation of these instruments will mostly directly image exoplanets in thermal emission (e.g. Quanz et al. 2015; Bowens et al. 2021), although instruments such as ELT/HARMONI and TMT/MODHIS might get to directly image some mature planets in reflected starlight (Houllé et al. 2021; Mawet et al. 2022). A next generation of ground-based direct-imaging instruments will be devoted to observing mature exoplanets in reflected starlight (Kasper et al. 2021; Fitzgerald et al. 2022; Males et al. 2022). ELTs will generally be sensitive to exoplanets around the nearest stars, some of them potentially down to Earth-like sizes (Kasper et al. 2021).

In space, the *Nancy Grace Roman Space Telescope*¹ (hereafter *Roman*, Spergel et al. 2015), planned for launch in late 2026 or early 2027, will be equipped with a Coronagraph Instrument observing at visible wavelengths (Kasdin et al. 2020). This instrument will directly image cold giant planets in reflected starlight (Carrión-González et al. 2021a) and also measure the thermal emission of young exoplanets (Lacy & Burrows 2020). *Roman*'s coronagraph will act as a technology demonstrator, paving the way for a next generation of missions, expected to directly image low-mass exoplanets down to the Earth-like regime in reflected starlight. With this goal, a Large IR/O/UV space telescope (recently named Habitable Worlds Observatory, HWO) was recommended to NASA as the next flagship mission by the US Astro 2020 Decadal Survey report (National Academies of Sciences Engineering and Medicine 2021). It combines some of the specifications of the LUVOIR² (Bolcar et al. 2016; The LUVOIR Team 2018) and HabEx³ (Mennesson et al. 2016; Gaudi et al. 2018) concepts proposed to the US Decadal Survey.

The Large Interferometer For Exoplanets (LIFE; Quanz et al. 2018, 2022b) is a complementary approach to HWO, proposed to directly image the thermal emission of low-mass temperate exoplanets in the mid-infrared. The mission concept consists of multiple free-flying telescopes operating together as a nulling interferometer in space. The mid-IR range is suitable to characterize the atmospheres of Earth-like exoplanets due to the

number of relevant molecules (e.g. H₂O, CO₂, O₃) with absorption bands at these wavelengths (Quanz et al. 2022a; Konrad et al. 2022; Alei et al. 2022; Angerhausen et al. 2023). This spectral range also provides a direct measurement of the planetary temperature and a strong constraint on its radius (Dannert et al. 2022). As such, mid-IR observations will overcome some of the physical degeneracies that affect the interpretation of reflected-starlight measurements, such as those caused by clouds and hazes (Lupu et al. 2016; Feng et al. 2018) or by an unknown planet radius (Carrión-González et al. 2020). Konrad et al. (2022) discussed the prospects for LIFE to retrieve the atmospheric structure and composition of an Earth analogue with different configurations of signal-to-noise ratio (S/N), spectral resolution (R), wavelength coverage and mirror size of each of the four collecting telescopes of the interferometer. They concluded that an accurate characterization could be achieved with a minimum wavelength coverage of 4–18.5 μm , $R = 50$, $S/N > 10$ and a mirror size of at least 2 m for a four-telescope configuration with a total 5% instrument throughput.

A key to understanding the scientific potential of a given direct-imaging mission is to determine the parameter space of exoplanets to which the telescope is most sensitive. Based on a synthetic population of exoplanets following occurrence rates from the *Kepler* mission, Kammerer & Quanz (2018) computed the possible exoplanet yield of a space-based mid-IR nulling interferometer and Quanz et al. (2022b) applied this methodology to the updated specifications of LIFE. An interferometer with four telescopes of 2 m aperture and 5% total throughput was found to yield more than 500 detectable exoplanets with planet radius $0.5 R_{\oplus} < R_p < 6 R_{\oplus}$ including between 10 and 20 exo-Earth candidates (more details in Table 1 of Quanz et al. 2022b). Kammerer et al. (2022) found that a configuration with four ~ 3 -m telescopes and 5% throughput (or four ~ 2 -m telescopes and 20% throughput) could detect about 30 rocky planets in the habitable zone of nearby Sun-like stars.

A different approach consists of using the current population of known exoplanets and determining the detectability of each planet with a given instrument, as done by Brown (2015) and Carrión-González et al. (2021a) for reflected-starlight missions. Although the set of known exoplanets remains biased due to the technology available – which is less sensitive to low-mass, long-period planets – this approach provides a catalogue of already-existing targets. This enables observational campaigns to improve the knowledge of their orbits and planetary systems, which will help in prioritizing targets.

Our goal in this work is to compute which of the currently known exoplanets are detectable with LIFE in the mid-IR. We also compute their detectability with a notional performance estimate for the HWO direct-imaging mission observing in reflected starlight. For that, we process the NASA Exoplanet Archive Database with the method described in Carrión-González et al. (2021a). We analyse the overlap of LIFE's exoplanet yield with that of HWO in reflected starlight and with transit surveys. This way we aim to provide a more concrete sense of the science cases that LIFE will be able to address, the targets that could benefit from multi-technique measurements, and those that are only detectable with LIFE. We focus on the population of exoplanets within 20 pc from the Sun, which is expected to offer better opportunities for detection and atmospheric characterization (Quanz et al. 2022b).

This paper is structured as follows. Section 2 summarizes the methodology to compute orbital realizations for each of the known exoplanets and determine their detectability both with LIFE in the mid-IR and with HWO in reflected starlight.

¹ Previously named Wide-Field Infrared Survey Telescope (WFIRST).

² Large UV/Optical/IR Surveyor.

³ Habitable Exoplanet Observatory.

Table 1. Summary of the parameters used in our computations.

Parameter	Unit	Description
d	pc	Distance to the star
R_{\star}	R_{\odot}	Stellar radius
M_{\star}	M_{\odot}	Stellar mass
T_{\star}	K	Stellar effective temperature
a	AU	Orbital semi-major axis of the planet
P	days	Orbital period
T_{eq}	K	Planet equilibrium temperature
R_{p}	R_{J}	Planet radius
M_{p}	M_{J}	Planet mass
i	deg	Orbital inclination
ω_{p}	deg	Argument of periastron of the planet
e	–	Orbital eccentricity

Section 3 describes the set of exoplanets detectable with LIFE and compares it with those accessible with HWO. This section also identifies the exoplanets detectable only with LIFE, those that are also observable in transit, and those in the habitable zone (HZ) of their host stars. The assumptions made throughout this work are discussed in Sect. 4, and Sect. 5 summarizes the main findings and conclusions.

2. Methods

Below we describe the statistical methodology used to simulate the orbits of the currently confirmed exoplanets and derive some relevant orbital and planetary parameters (Sect. 2.1). Then, in Sects. 2.2 and 2.3 we evaluate the detectability prospects of each planet with LIFE and with a reflected-starlight telescope.

2.1. Simulated orbital realizations

Following the methodology in Carrión-González et al. (2021a), we downloaded the information of the known exoplanets from the NASA Exoplanet Archive⁴ (Akeson et al. 2013). We used the Default Parameter Set in the NASA Exoplanet Archive’s Planetary Systems database as of November 6, 2022, containing a total of 5197 confirmed exoplanets of which 259 are closer than 20 pc. For some exoplanets we complemented this information with data from the original references therein, the Composite database of the NASA Exoplanet Archive or the Extrasolar Planets Encyclopaedia⁵ (Schneider et al. 2011), as indicated in the text.

For each exoplanet, we computed 1000 orbital realizations by randomly varying the orbital parameters (Table 1) within the uncertainties reported in the NASA Exoplanet Archive. In those cases where the orbital information of a planet was incomplete, we used statistical arguments to have a complete description of the orbit. For instance, we assumed isotropically distributed orbital orientations when the values of the orbital inclination (i) or the argument of periastron of the planet⁶ (ω_{p}) were not

⁴ <https://exoplanetarchive.ipac.caltech.edu>

⁵ <http://exoplanet.eu>

⁶ We assumed that the reported values of the argument of periastron in the NASA Exoplanet Archive correspond to those of the star (ω_{\star}) because that is the usual convention for radial velocity (RV) detections (see e.g. Householder & Weiss 2022). We refer to Sect. 4.1.1 in Carrión-González et al. (2021a) for an additional discussion on the lack of a homogeneous convention in reporting ω and the relevance of this for accurately computing the detectability prospects.

available. In those cases we thus randomly drew values at each orbital realization from the uniform distributions $\cos(i) \in [-1, 1]$ and $\omega_{\text{p}} \in [0, 2\pi]$ respectively. With this we obtained a value of the planet mass (M_{p}) for each orbital realization even if only the minimum mass $M_{\text{p}} \sin(i)$ was available in the NASA Exoplanet Archive. If the orbital eccentricity (e) was unknown we assumed a uniform probability distribution $e \in [0, 1)$. In case of an unknown planet radius (R_{p}) we computed it for each simulated orbit by means of previously published mass-radius relationships (Hatzes & Rauer 2015; Otegi et al. 2020). We refer to Sect. 4.2 in Carrión-González et al. (2021a) for more information on the implementation of these relationships.

We discretize each orbital realization into 360 points evenly spaced in orbital true anomaly, and we compute the equilibrium temperature of the planet (T_{eq}) at each orbital position:

$$T_{\text{eq}} = \left(\frac{1 - A_{\text{B}}}{4f} \right)^{1/4} \left(\frac{R_{\star}}{r} \right)^{1/2} T_{\star}. \quad (1)$$

Here, R_{\star} is the stellar radius, T_{\star} is the stellar effective temperature, r is the distance between the planet and the star at that orbital position and A_{B} is the Bond albedo of the planet. We fix $A_{\text{B}} = 0.45$ for all planets to be consistent with our assumption of geometrical albedo $A_{\text{g}} = 0.3$ and Lambertian scattering (see Sect. 2.3). f is a factor related to the heat redistribution of the planet for which we assume $f = 1$, consistent with fast-rotating planets that have efficient heat redistribution (Traub & Oppenheimer 2010).

In the cases where the values of M_{\star} , R_{\star} , or T_{\star} were not available in the default parameter set of the NASA Exoplanet Archive, we obtained them from SWEET-Cat (Santos et al. 2013; Sousa et al. 2021). When not available here either, we adopted the values reported in the NASA Archive from the *Gaia* DR2 (Gaia Collaboration 2018) or the Revised TESS Input Catalog (Stassun et al. 2019). In less than 1% of cases, no values were to be found for these parameters and we excluded these planets from our analysis.

From this bootstrap-like method we derive statistical conclusions for the sampled parameters of each exoplanet. In Table G.1 we report the median values of the corresponding posterior distributions and their 16% and 84% confidence intervals (1σ for Gaussian distributions), as resulting from our methodology, for all exoplanets within 20 pc.

2.2. Detectability with LIFE

In this work we assume for LIFE an architecture consisting of a rectangular interferometric array with four free-flying telescopes sending their light to a fifth beam combiner spacecraft. Nulling of the central source (here the host star) is achieved with a dual chopped Bracewell beam combination scheme (Lay 2004). This architecture is particularly suitable for the suppression and self-calibration of instrumental noise as outlined in Dannert et al. (2022). We note that novel approaches such as three or five telescope kernel-nullers and their potential impact on the science return of a mission such as LIFE have been investigated in Hansen et al. (2022, 2023).

The integration time (t_{int}) required to detect a given planet is calculated using LIFESim (Dannert et al. 2022), which considers astrophysical noise sources such as stellar leakage, local zodiacal, and exozodiacal light, but does not account for instrumental noise sources as yet. This approach is only valid if LIFE is operated in a photon noise-dominated regime and Appendix C of Dannert et al. (2022) derives the minimum requirements on

instrumental amplitude, phase, polarization, and spacecraft positioning errors to be operating in such a regime. We note that previous studies (Quanz et al. 2022b; Kammerer et al. 2022) have assumed a conservative signal-to-noise ratio (S/N) of 7 (integrated over the full wavelength range) for a planet to be regarded as a detection to budget in additional instrumental noise. We adopted the same criterion in this work and assumed as detectable with LIFE any exoplanet for which an integrated $S/N = 7$ is achieved in less than 100 h of integration time.

For each known exoplanet, we provided LIFESim with the following planetary and stellar parameters as inputs: planetary radius and equilibrium temperature, planet-star separation, distance to the planetary system and its ecliptic coordinates, and radius and effective temperature of the star. The planetary parameters correspond to the median values obtained with our methodology (Table G.1) and the stellar parameters are obtained from the NASA Archive as indicated in Sect. 2.3. In each case, we assumed the optimal instrument baseline that maximizes throughput at the angular separation of the planet semi-major axis. This is motivated by the fact that the considered planets are already known so that the observations can in principle be scheduled optimally. In all cases, the nulling interferometry baseline length ranges between 10 and 100 m.

We note that the effective temperature of a planet may be higher than the T_{eq} reported here due to, for instance, internal heat sources. These effects, are especially relevant for young exoplanets. Also, Solar System planets have shown that cold, mature giant planets can have internal heat sources resulting in effective temperatures significantly higher than the T_{eq} (e.g. Li et al. 2018). This will increase the planet brightness in the mid-IR. A case-by-case analysis is needed, as the outcome is highly dependent on the evolutionary models and atmospheric properties assumed. Such analysis of the evolution of each particular planet is out of the scope of this work.

For our calculations, we consider three different scenarios to account for uncertainties in the instrumental parameters of LIFE. We consider mirror diameters of 1 m (pessimistic), 2 m (reference), and 3.5 m (optimistic) with their corresponding wavelength coverage of 6–17, 4–18.5, and 3–20 μm that will be adopted implicitly throughout this work. Table 2 summarizes the mission parameters adopted for LIFE. We refer to Quanz et al. (2022b) and Dannert et al. (2022) for a more comprehensive discussion of their meaning and assumed values. Furthermore, we set the exozodiacal dust level to 3 zodi for all exoplanetary systems, motivated by the results from the HOSTS survey (Ertel et al. 2020). In Sect. 4, we discuss the effects of assuming other values of exozodiacal dust.

For simplicity, we consider all stellar hosts as single. However, out of the 149 exoplanet-hosting stars within 20 pc, 30 of them – hosting a total of 49 exoplanets – are multiples. Planets whose hosts are multiples might require longer integration times than what is shown here or might not be possible to be observed with LIFE at all (see details in Sect. 4). This will require detailed analyses for each case, to be done in future work.

2.3. Detectability with reflected-starlight telescopes

Future direct imaging missions will achieve reflected-starlight observations of exoplanets in the visible and near-IR range by suppressing the stellar glare of the host star using devices such as coronagraphs or starshades. Unavoidably, part of the inner region of the planetary system is obscured together with the host star, as defined by the inner working angle (IWA) of the instrument.

Table 2. LIFE mission parameters adopted for the exoplanet yield predictions.

Parameter		Value	Unit
Number of collector spacecraft		4	–
Mirror diameter	pessimistic	1.0	m
"	reference	2.0	m
"	optimistic	3.5	m
Wavelength coverage	pessimistic	6.0–17.0	μm
"	reference	4.0–18.5	μm
"	optimistic	3.0–20.0	μm
Spectral resolution		20	$\lambda/\Delta\lambda$
Min. nulling baseline length		10	m
Max. nulling baseline length		100	m
Ratio imaging/nulling baseline		6	–
Quantum efficiency		0.7	–
Throughput		0.05	–
S/N_{target}		7	–

Similarly, these instruments have an outer working angle (OWA) that defines the outer limit of the detectable region. Beyond that, diffracted light from the suppression device reduces the contrast significantly. In addition, the detectability is also limited by the minimum contrast of the instrument (C_{min}), such that the planet has to be brighter than C_{min} in order to be distinguished from speckles and other noise.

The population of exoplanets accessible in reflected starlight is thus primarily defined by the IWA, the OWA, and C_{min} . In this work, we considered these three parameters as the main detectability criteria for reflected-starlight observations. Lacking an official list of specifications for the Habitable Worlds Observatory, we assumed notional values of IWA, OWA, and C_{min} based on the Decadal Survey report and the LUVOIR and HabEx proposals. Throughout this work, we assume a telescope diameter $D = 6$ m, $\text{IWA} = 3 \lambda/D$, $\text{OWA} = 64 \lambda/D$, and $C_{\text{min}} = 10^{-10}$. We note, however, that a detailed instrument design and corresponding performance predictions for HWO are still work in progress.

For each orbital realization of a given exoplanet, we computed at each orbital position the angular separation ($\Delta\theta$) between the planet and the host star, and the planet brightness in reflected starlight given by the planet-to-star contrast ratio (F_p/F_\star). We refer to Sect. 3 in Carrión-González et al. (2021a) for more details on the computations. In this work, we adopt a reference wavelength of $\lambda = 575$ nm for all reflected starlight observations and a geometric albedo of $A_g = 0.3$ for all exoplanets, with a Lambertian scattering phase law.

The orbital positions that are potentially observable in reflected starlight are hence those with $\Delta\theta$ between the IWA and the OWA, and F_p/F_\star greater than C_{min} . If these two criteria are simultaneously met, we refer to that exoplanet as accessible to the reflected-starlight mission under consideration. The probability of the planet to be accessible to that mission (P_{access}) is the ratio between the number of orbital realizations in which the planet is accessible and the total number of 1000 simulations.

Additional factors will also play a role in the detectability of exoplanets directly imaged in reflected starlight. For instance, zodiacal and exozodiacal light might prevent the detection of certain targets. The mission schedule and the pointing of the telescope will also restrict in practice the systems that can be observed at a given time (Brown 2015), although full sky coverage can be expected throughout a year for observatories

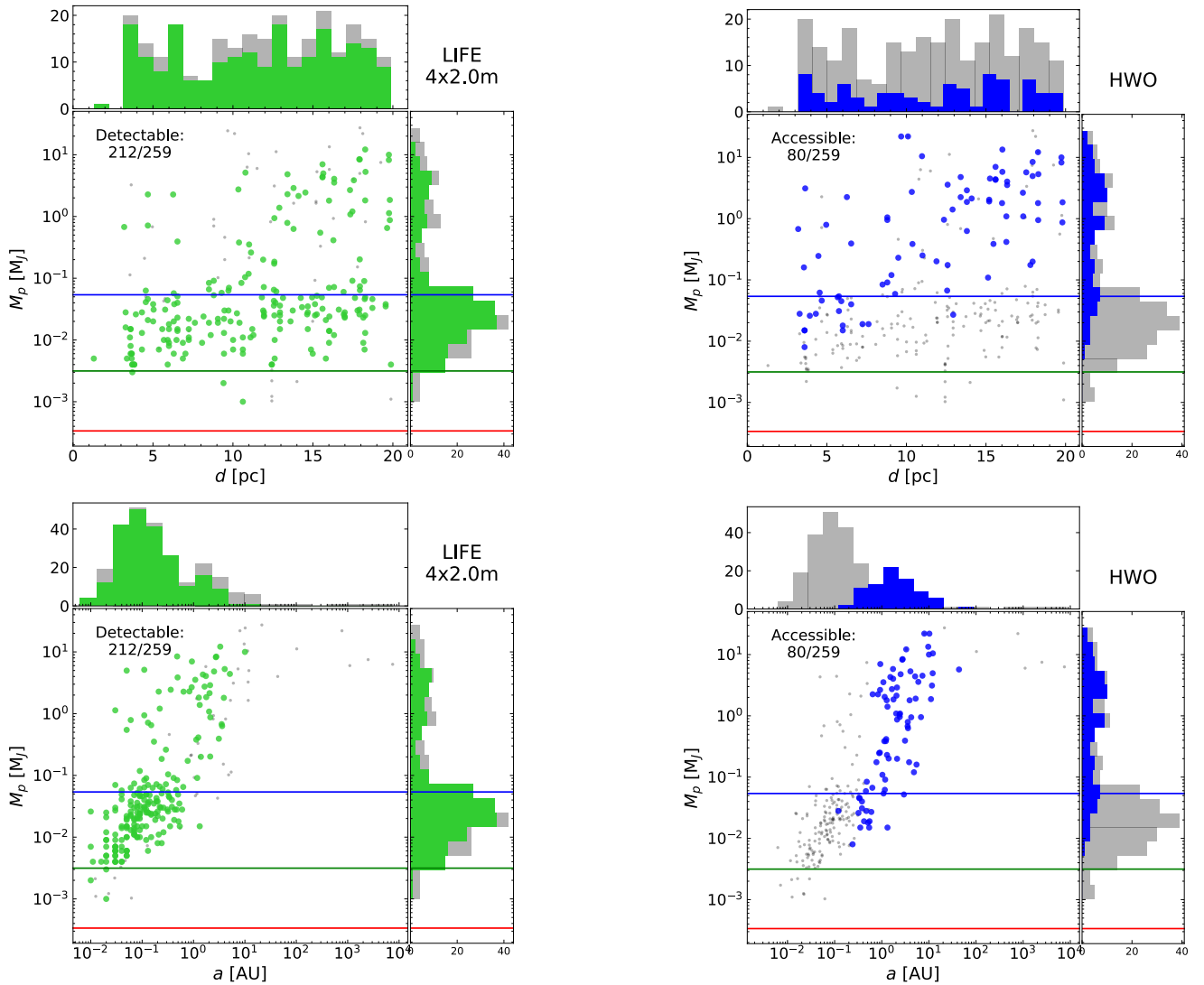


Fig. 1. Potentially detectable currently-known exoplanets (coloured circles and histograms) compared to the total population of known exoplanets within 20 pc (grey dots and histograms), shown both as a function of their distance to the Solar System (top row) and their semimajor axis (bottom row). For LIFE (green), we assume the reference 4×2 m configuration with 5% throughput and consider planets as detectable if $t_{\text{int}}(S/N = 7) < 100$ h. For the notional HWO (blue), potential targets in reflected starlight are those that meet our IWA, OWA and C_{min} requirements (Sect. 2.3) and have $P_{\text{access}} > 25\%$. In all subplots, the value of M_p reported for the potential targets is the output of our statistical methodology (Sect. 2.1). For the non-detectable exoplanets we plot M_p or alternatively $M_p \sin i$ as reported in the NASA Archive. Horizontal lines indicate the masses of Neptune (blue), Earth (green) and Mars (red).

located at the Earth-Sun L2 point. The optical magnitude of the host star might affect the performance of the instrument and even prevent the observations of planets with faint host stars. We also note that speckle subtraction techniques might improve the C_{min} up to a factor of about 2.5 (e.g. Ygouf et al. 2016). Evaluating the impact of these higher-order effects requires, however, a case-by-case analysis based on follow-up observations of each planet and instrument-specific tools to simulate the scheduling and the noise budget. For this reason we generally use IWA, OWA, and C_{min} as our main detectability criteria.

3. Results

We show here the currently known planets within 20 pc that are detectable with LIFE, discussing the common targets for LIFE and HWO (Sect. 3.1) as well as those that are only detectable with LIFE and not accessible with HWO in reflected starlight (Sect. 3.2). Some of the planets detectable with LIFE have

already been observed in transit and we comment on these in Sect. 3.3. In Sect. 3.4, we identify the exoplanets detectable with LIFE which orbit within the habitable zone of their host star. Appendix F shows the integration times required to detect with LIFE the young exoplanets that have been directly imaged to date.

3.1. Synergies with reflected-starlight space missions

Observing an exoplanet both at visible wavelengths and in the mid-IR will provide unique information about the planet and its atmosphere. Visible, reflected-starlight observations are particularly sensitive to the optical properties of the clouds (optical thickness, particle size and composition, Garcia Muñoz & Isaak 2015), which provide key information on the meteorological phenomena taking place in the planet. On the other hand, clouds trigger multiple degeneracies between physical parameters, hindering the interpretation of the measurements

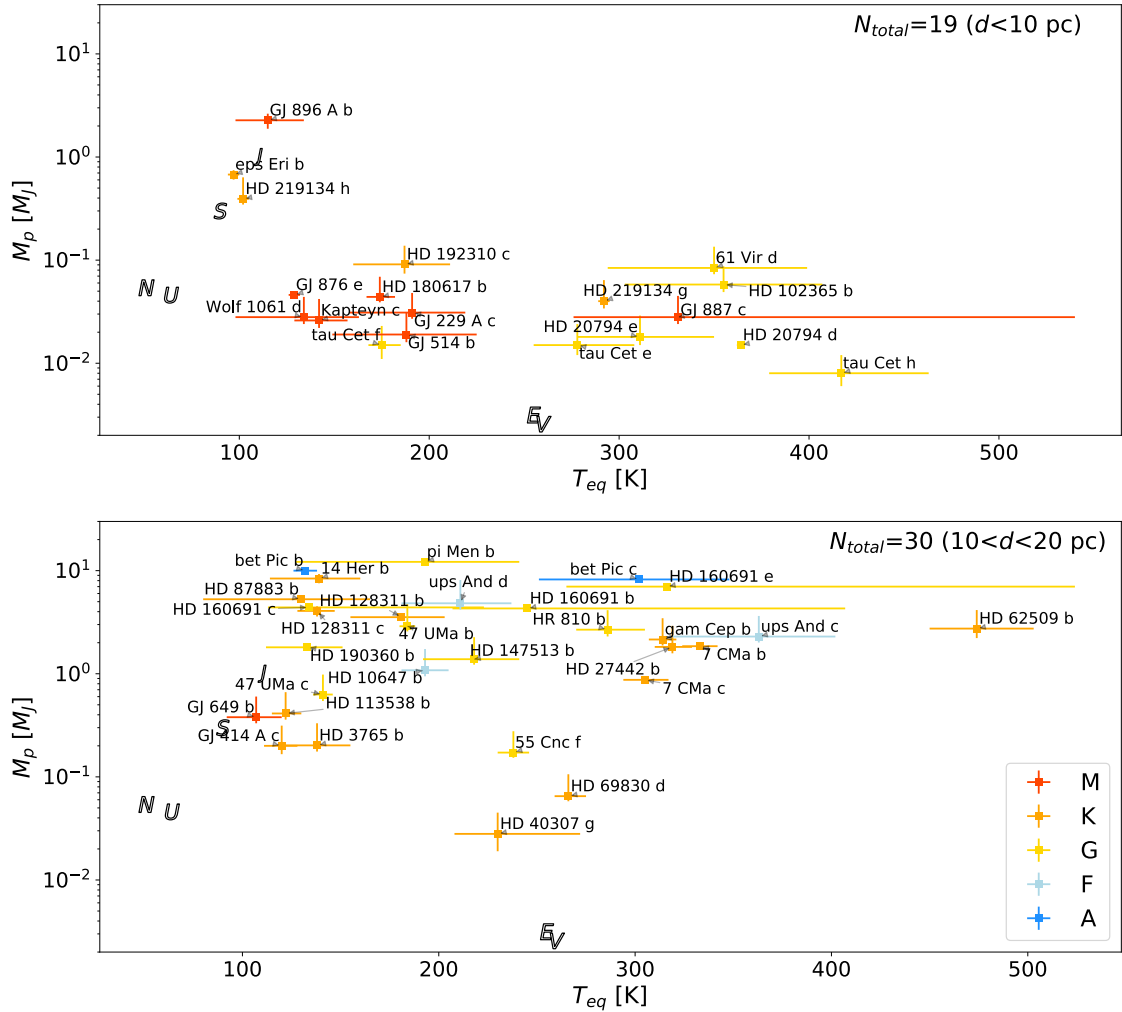


Fig. 2. Equilibrium temperatures and planet masses estimated for each of the currently-known exoplanets that are common targets for LIFE’s reference configuration and the notional HWO. Each planet is colour-coded according to its host-star spectral type, as indicated in the legend. The top panel shows the common targets closer than 10 pc and the bottom panel shows those between 10 and 20 pc. M_p and T_{eq} are the median values computed from the 1000 orbital realizations (Sect. 2.3), with error bars corresponding to the upper and lower uncertainties (16% and 84% percentiles). Indicated with black letters are the Solar-System planets Venus (V), Earth (E), Jupiter (J), Saturn (S), Uranus (U), and Neptune (N).

(Nayak et al. 2017; Feng et al. 2018; Damiano & Hu 2020; Carrión-González et al. 2021b). The optical properties of the clouds are also highly degenerate with the value of the planet radius, if it is unknown (Carrión-González et al. 2020). If these parameter degeneracies are overcome, the visible wavelength range contains spectral features relevant to habitability studies, such as the ocean glint (Williams & Gaidos 2008; Lustig-Yaeger et al. 2018) or the vegetation’s red edge (Sagan et al. 1993; Seager et al. 2005). The mid-IR is less sensitive to the clouds and in principle offers less insight into their properties, but on the positive side it is less affected by the cloud-related degeneracies. In general, the mid-IR can probe deeper down in the atmosphere and determine the temperature profile and the abundance of gaseous species (Quanz et al. 2022a; Konrad et al. 2022; Alei et al. 2022; Angerhausen et al. 2023), several of which are potential biomarkers (Schwieterman et al. 2018).

Figure 1 shows the known exoplanets within 20 pc that are potential targets for LIFE and HWO, computed with the methodology described in Sect. 2. Planets are considered detectable by LIFE if they have $t_{int} < 100$ h and they are considered accessible with HWO in reflected starlight if they meet $P_{access} > 25\%$. A very high spatial resolution interferometric mission such as LIFE is particularly well suited to detect exoplanets orbiting

at small separations. This makes LIFE especially sensitive to the currently-known low-mass exoplanets, which have generally been found at small orbital separations due to current observational biases. Indeed, LIFE can detect 144 of the 161 known planets (89%) with $M_p < M_{Neptune}$ within 20 pc, and 68 of the 98 planets (69%) with $M_p > M_{Neptune}$. Reflected-starlight missions are less sensitive to the currently known low-mass planets. The accessible planets within 20 pc for HWO are 16 with $M_p < M_{Neptune}$ (10%) and 64 with $M_p > M_{Neptune}$ (65%). The reason for this is that most of the low-mass nearby planets discovered to date orbit M-type stars in short-period orbits which fall within the IWA of optical coronagraphs. This gap in the parameter space of currently-discovered exoplanets is clearly shown in the bottom row of Fig. 1.

Figure A.1 extends Fig. 1 to show the planets beyond 20 pc accessible with HWO in reflected starlight. Our criteria to deem a planet accessible in reflected starlight (IWA, OWA, C_{min}) are mostly geometrical and thus less restrictive than those to deem a planet detectable with LIFE, because LIFEsim includes additional noise sources and instrument sensitivity. Based on these geometrical considerations, we find a large number of long-period giant planets accessible to HWO out to about 100 pc (Fig. A.1). Whether these targets will be actually detectable

Table 3. Detectability of the exoplanets within 20 pc with the notional HWO mission in reflected starlight and LIFE in emitted light, computed with the methods in Sect. 2.

Planet	d (pc)	a (AU)	R_p (R_\oplus)	M_p (M_\oplus)	T_{eq} (K)	Notional HWO	LIFE (4x1m)		LIFE (4 × 2 m)		LIFE (4 × 3.5 m)	
						P_{access} (%)	S/N (10 h)	t_{int} (h)	S/N (10 h)	t_{int} (h)	S/N (10 h)	t_{int} (h)
tau Cet h	3.60	0.24	1.35	2.54	417	100.0	41	0.3	107	0.04	219	0.01
tau Cet f	3.60	1.32	1.91	4.77	175	100.0	–	–	7	11	18	2
tau Cet e	3.60	0.54	1.91	4.77	278	100.0	25	0.8	77	0.08	174	0.02
HD 20794 d	6.00	0.35	1.91	4.77	364	100.0	26	0.7	73	0.09	156	0.02
HD 20794 e	6.00	0.51	2.24	5.72	311	100.0	23	1.0	69	0.1	153	0.02
GJ 514 b	7.62	0.42	2.35	6.04	188	99.8	–	–	7	10	23	0.9
Kapteyn c	3.93	0.32	2.80	8.26	142	100.0	–	–	8	7	29	0.6
HD 40307 g	12.94	0.60	2.80	8.90	230	32.2	3	68	11	4	31	0.5
GJ 887 c	3.29	0.12	2.91	8.90	331	45.7	155	0.02	488	0.002	1132	0.0004
Wolf 1061 d	4.31	0.47	2.91	8.90	134	100.0	–	–	4	29	15	2
GJ 229 A c	5.76	0.38	3.14	9.85	191	100.0	6	13	26	0.7	82	0.07
HD 219134 g	6.53	0.38	3.59	12.71	292	100.0	42	0.3	138	0.03	329	0.005
HD 180617 b	5.91	0.34	3.92	13.98	174	100.0	5	20	22	1	69	0.1
GJ 876 e	4.68	0.33	3.92	14.62	129	100.0	–	–	5	21	18	2
HD 102365 b	9.29	0.46	4.60	18.43	355	87.6	69	0.1	214	0.01	485	0.002
HD 69830 d	12.56	0.63	5.04	20.66	266	100.0	16	2	60	0.1	160	0.02
61 Vir d	8.50	0.48	5.83	26.70	350	100.0	119	0.03	369	0.004	842	0.0007
HD 192310 c	8.80	1.18	6.05	28.92	187	100.0	7	9	31	0.5	92	0.06
GJ 414 A c	11.89	1.39	8.86	63.56	120	100.0	–	–	2	83	9	6
55 Cnc f	12.58	0.77	9.19	54.66	238	100.0	30	0.6	115	0.04	319	0.005
HD 3765 b	17.93	2.11	10.09	64.20	138	100.0	–	–	4	32	14	3
pi Men b	18.27	3.31	11.77	3866.24	193	100.0	8	9	33	0.5	105	0.04
HD 160691 e	15.60	0.93	12.11	2224.72	316	100.0	126	0.03	421	0.003	1011	0.0005
14 Her b	17.93	2.77	12.11	2665.84	139	100.0	–	–	7	11	24	0.9
HD 87883 b	18.29	4.04	12.33	1677.75	130	100.0	–	–	3	75	10	5
ups And d	13.41	2.51	12.33	1533.15	211	100.0	26	0.7	97	0.05	255	0.008
HD 160691 b	15.60	1.52	12.44	1366.61	245	100.0	44	0.3	166	0.02	436	0.003
HD 128311 c	16.33	1.74	12.44	1293.20	138	100.0	–	–	7	10	24	0.8
HD 160691 c	15.60	5.10	12.44	1398.39	134	100.0	–	–	5	24	16	2
HD 128311 b	16.33	1.08	12.55	1124.43	181	100.0	8	7	36	0.4	118	0.04
47 UMa b	13.79	2.10	12.67	918.49	184	100.0	13	3	54	0.2	155	0.02
HR 810 b	17.32	0.92	12.67	850.48	286	100.0	81	0.08	282	0.006	702	0.001
HD 62509 b	10.34	1.64	12.67	871.45	474	100.0	144	0.02	334	0.004	654	0.001
gam Cep b	14.10	2.05	12.78	682.99	314	100.0	87	0.06	229	0.009	477	0.002
ups And c	13.41	0.83	12.78	729.39	363	100.0	255	0.008	742	0.0009	1600	0.0002
GJ 896 A b	6.26	0.64	12.89	721.76	115	100.0	3	77	13	3	51	0.2
HD 190360 b	16.01	3.89	13.00	573.66	133	100.0	–	–	5	20	19	1
HD 27442 b	18.27	1.27	13.00	578.74	319	100.0	84	0.07	246	0.008	539	0.002
7 CMa b	19.81	1.77	13.00	588.28	333	100.0	65	0.1	180	0.02	380	0.003
HD 147513 b	12.90	1.32	13.11	439.86	218	100.0	38	0.3	150	0.02	416	0.003
HD 10647 b	17.34	2.01	13.23	343.56	193	100.0	13	3	54	0.2	156	0.02
7 CMa c	19.81	2.12	13.45	277.45	305	100.0	55	0.2	158	0.02	344	0.004
bet Pic c	19.75	2.72	13.45	2610.86	302	100.0	73	0.09	214	0.01	466	0.002
47 UMa c	13.79	3.60	13.67	199.91	141	100.0	2	93	11	4	40	0.3
eps Eri b	3.20	3.53	13.67	214.84	97	100.0	–	–	9	7	30	0.6
HD 113538 b	16.28	1.24	13.90	130.94	122	100.0	–	–	4	31	15	2
HD 219134 h	6.53	3.11	14.01	124.90	102	100.0	–	–	5	19	18	2
GJ 649 b	10.38	1.13	14.01	120.45	107	100.0	–	–	4	35	14	2
bet Pic b	19.75	10.02	18.49	3175.94	132	100.0	–	–	6	12	19	1

Notes. For HWO, we include only planets with $P_{\text{access}} > 25\%$. For LIFE, we list both the t_{int} required to achieve a detection (i.e. $S/N = 7$) as well as the S/N achieved in 10 h. Integration times longer than 100 h are not shown.

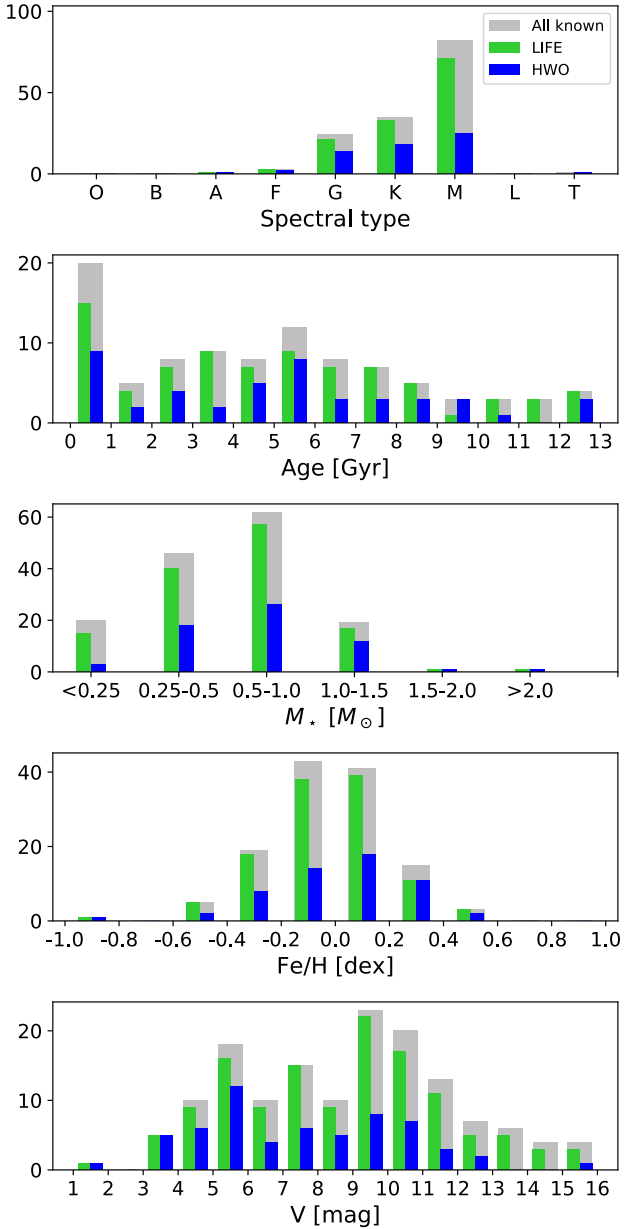


Fig. 3. Stellar properties reported in the NASA Exoplanet Archive for the hosts of the LIFE-detectable exoplanets (4×2 m and 5% throughput) and those accessible in reflected-starlight with the notional HWO within 20 pc. Shown in grey for comparison, the stellar properties of the 149 stars hosting currently-known exoplanets within 20 pc. Out of these 149 stars, 97% have available information on the spectral type, 63% on the stellar age, 100% on the stellar mass (M_*), 85% on the stellar metallicity, and 100% on the optical magnitude (V). A total of 116 stars host LIFE-detectable exoplanets (resp. 61 for HWO).

will depend on the final operational and performance specifications of the mission and its sensitivity limits, which are not yet defined. Nevertheless, the number of low-mass planets accessible in reflected starlight beyond 20 pc does not increase from those in Fig. 1.

Table 3 shows the list of 49 exoplanets within 20 pc that are detectable with LIFE’s reference configuration and are also accessible with the notional HWO mission in reflected starlight. Figure 2 provides additional information on the equilibrium temperature and mass of these planets. We find that most of the planets that are common targets for LIFE and HWO are cold and temperate giant planets, with masses similar to that

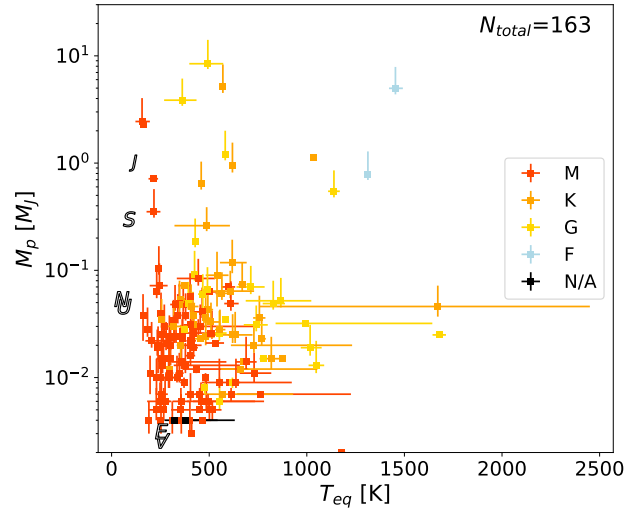


Fig. 4. Equilibrium temperatures and planet masses estimated for each of the known exoplanets within 20 pc that are detectable with LIFE (4×2 m and 5% throughput) but not with the notional HWO. Colour-coding corresponds to the host-star spectral type. Table D.1 contains the list of planets and their properties.

of Jupiter and equilibrium temperatures between that of Jupiter and that of the Earth. Within 10 pc, some planets less massive than Neptune are accessible for both LIFE and HWO, including the low-mass planets tau Cet e, f and h, HD 20794 d and e, and GJ 514 b.

Figure 3 compares the properties of the stars within 20 pc hosting potential targets for the notional LIFE and HWO missions. Among the known exoplanet-hosts, LIFE can study planetary systems with hosts of practically all stellar types and masses, and especially with stars less massive than the Sun. The information on stellar age and metallicity is scarcer in the NASA Archive (e.g. only available for 59% and 87% of LIFE-detectable-planet hosts, respectively). However, we find that LIFE may analyse a significant number of planets orbiting stars of almost any age or metallicity value. We note that M-type stars frequently lack an exact value of their age in the NASA Archive, which especially affects the tally of LIFE-detectable-planet hosts. LIFE’s mid-IR wavelength range also makes it more sensitive to stars that are dim in the visible ($V \geq 9$ mag). The V magnitude of a star will be a limiting factor for the detectability of exoplanets with reflected-starlight missions, as indicated in Sect. 2.3.

The exoplanets discussed in this section are valuable candidates for an in-depth atmospheric characterization spanning a broad range of wavelengths. In addition, large numbers of planets are expected to be discovered in the coming years and decades with ongoing and upcoming transit and radial-velocity instruments. As shown in Fig. 1, LIFE performs well over a broad parameter space and will be able to detect a significant fraction of these newly discovered targets. The particularly interesting cases of temperate long-period planets around nearby Sun-like stars will generally be accessible both with LIFE and with HWO in reflected starlight. The number of overlapping targets is thus expected to increase in the near future.

3.2. Unique parameter space for LIFE

The nulling interferometry method allows LIFE to detect planets on short-period orbits that cannot be resolved with optical coronagraphs or starshades. Also, with temperate exoplanets’ thermal emission peaking in the mid-IR, LIFE is more sensitive to low-mass planets that might not reflect enough light to be

detectable in the visible. Figure 4 shows the 163 known exoplanets within 20 pc that can only be detected with LIFE’s reference configuration and not with HWO in reflected starlight. Table D.1 displays additional details on the main properties of these planets. Figure B.1 shows the 31 known exoplanets within 20 pc accessible in reflected starlight to the notional HWO but not detectable with LIFE’s reference configuration –giant planets with low T_{eq} which do not emit enough thermal radiation to allow a detection in the mid-IR.

In the reference LIFE configuration (4×2 m telescopes with 5% throughput), only eight of these 163 planets require integration times longer than 10 h to be detected with a S/N of 7. Among the targets only detectable by LIFE, we find 62 exoplanets with masses $M_p < 5M_{\oplus}$. Of these low-mass planets, 37 require 1 h of integration or less in order to achieve a detection with $S/N = 7$ in the reference configuration. Figure C.1 shows the t_{int} of each LIFE-detectable exoplanet.

The variety of exoplanets only detectable with LIFE ranges from hot Jupiters (e.g. 51 Peg b) to temperate planets with similar mass to that of the Earth (e.g. Teegarden’s Star b and c). The host stars of these exoplanets also range from stars more massive than the Sun down to M dwarfs. Below we comment in more detail on the planets detectable with LIFE which have also been detected in transit (Sect. 3.3) and those that orbit within the habitable zone of their host star (Sect. 3.4).

3.3. Transiting planets detectable with LIFE

As of November 6, 2022, 40 of the known exoplanets within 20 pc have been found to transit their host stars. These planets are listed in Table 4 together with the integration times required to detect them with different configurations of LIFE.

LIFE will be able to detect 32 of these transiting planets with $t_{\text{int}} < 100$ h in the reference 4×2 m configuration with 5% throughput. This is a result of the high angular resolution achievable with a space-based mid-IR interferometer. None of these 40 planets is accessible with HWO in reflected starlight due to their small orbital separations.

The LIFE-detectable transiting planets in Table 4 are mainly warm and hot ($T_{\text{eq}} \sim 500\text{--}700$ K) short-period planets in the super-Earth to Neptune-like mass regime. Several hotter planets are also detectable, such as the hot-Jupiter HD 189733 b ($T_{\text{eq}} = 1036$ K) and the super-Earths 55 Cnc e ($T_{\text{eq}} = 1678$ K) and pi Men c ($T_{\text{eq}} = 1006$ K). These planets orbit too close to their host stars to be resolved by optical coronagraphs.

Multi-planet systems are valuable case studies to understand planetary systems as a whole and to constrain the possible formation and evolution of the planets. We find several systems with more than one transiting planet detectable with LIFE. These are HD 219134 (b, c), L 98-59 (b, c, d), HD 136352 (b, c, d), GJ 143 – also named HD 21749 – (b, c), HD 260655 (b, c), LTT 1445 A (b, c), AU Mic (b, c), and TRAPPIST-1 (b, c). Several other multi-planet systems with one or no transiting planets are also detectable with LIFE, as shown in Tables 3 and D.1.

Among these known transiting planets, the only ones in the habitable zone of their host star are LHS 1140 b and TRAPPIST-1 e, f, g. Although these planets are interesting for habitability studies (see e.g. Wunderlich et al. 2021), their t_{int} are beyond our detectability criteria even for LIFE’s optimistic configuration. This is due to the extremely small angular separation of these planets around stars of very low mass (e.g. 1.6 and 2.4 milliarcseconds for TRAPPIST-1 e and f, respectively). The nulling baseline length needed to optimally resolve these planets is larger than the maximum baseline length of 100 m assumed in

Table 4. Integration times required to detect with $S/N = 7$ the known transiting exoplanets within 20 pc, for each of the LIFE configurations assuming a total 5% throughput in all cases.

Planet	d (pc)	a (AU)	R_p (R_{\oplus})	4×1 m (h)	4×2 m (h)	4×3.5 m (h)
HD 189733 b	19.76	0.03	12.67	0.004	0.0003	6e-05
GJ 436 b	9.75	0.03	4.15	0.02	0.003	0.0008
AU Mic b	9.72	0.06	4.71	0.02	0.004	0.001
HD 219134 b	6.53	0.04	1.57	0.1	0.02	0.006
HD 219134 c	6.53	0.07	1.46	0.2	0.03	0.01
HD 136352 c	14.68	0.17	2.91	0.2	0.03	0.007
AU Mic c	9.72	0.11	2.91	0.2	0.02	0.004
HD 136352 b	14.68	0.10	1.68	0.7	0.1	0.03
GJ 357 b	9.44	0.04	1.23	0.9	0.1	0.02
pi Men c	18.27	0.07	1.79	1	0.1	0.04
55 Cnc e	12.59	0.02	1.91	1	0.09	0.02
LTT 1445 A c	6.87	0.03	1.12	1	0.2	0.03
HD 260655 c	10.01	0.05	1.57	1	0.2	0.04
GJ 486 b	8.07	0.02	1.35	1	0.2	0.04
LTT 1445 A b	6.87	0.04	1.35	2	0.2	0.05
GJ 143 b	16.32	0.19	2.58	3	0.3	0.05
HD 260655 b	10.01	0.03	1.23	3	0.4	0.1
HD 136352 d	14.68	0.43	2.58	4	0.4	0.07
HD 21749 c	16.32	0.07	0.90	6	0.8	0.2
L 98-59 d	10.62	0.05	1.57	11	1	0.2
L 98-59 c	10.62	0.03	1.35	14	1	0.3
LHS 3844 b	14.88	0.01	1.35	26	0.3	0.05
GJ 1132 b	12.61	0.02	1.12	42	2	0.4
L 98-59 b	10.62	0.02	0.90	51	4	1
GJ 367 b	9.41	0.01	0.67	63	5	1
LHS 1478 b	18.23	0.02	1.23	105	2	0.5
GJ 1214 b	14.64	0.01	2.69	157	4	0.8
GJ 3929 b	15.81	0.03	1.12	165	9	2
LHS 1678 c	19.88	0.03	1.01	1116	50	10
LHS 1140 c	14.99	0.03	1.12	1158	51	8
TRAPPIST-1 c	12.43	0.016	1.12	2202	73	10
TRAPPIST-1 b	12.43	0.011	1.12	4558	97	15
TOI-540 b	14.00	0.01	0.90	7493	146	32
LHS 1678 b	19.88	0.01	0.67	13 588	238	52
LHS 1140 b	14.99	0.10	1.68	44 160	2596	268
TRAPPIST-1 e	12.43	0.029	0.90	83 523	4681	526
TRAPPIST-1 d	12.43	0.022	0.78	100 405	4712	575
TRAPPIST-1 f	12.43	0.038	1.01	115 282	6872	736
TRAPPIST-1 g	12.43	0.047	1.12	132 300	7835	813
TRAPPIST-1 h	12.43	0.062	0.78	–	166 656	16 422

this work (Table 2)⁷. The observation of these planets cannot be optimized, resulting in a significant stellar leakage that prevents a detection in $t_{\text{int}} < 100$ h. Indeed, we verified that t_{int} drops to about 100 h for these planets with a nulling baseline of 500 m.

The list of transiting exoplanets will grow in the next years with missions monitoring nearby systems such as TESS and PLATO. These missions will discover long-period transiting planets accessible to LIFE and also to reflected-starlight imaging telescopes, constraining the value of their radius. Nearby transiting exoplanets will also be targeted by JWST and Ariel, and many of those in Table 4 will be thoroughly studied in the

⁷ We recall that the first positive transmission peak in the nulling interferometer is proportional to the nulling baseline b , $\lambda/2b$, while for a single-mirror telescope the spatial resolution is proportional to the mirror diameter D , λ/D (see e.g. Dannert et al. 2022).

coming years. Several of them have been observed with ground-based high-resolution Doppler spectroscopy (e.g. Bourrier et al. 2022; López-Morales et al. 2014; Wyttenbach et al. 2015). It thus unlikely that planets in Table 4 will be prime targets for LIFE, although they illustrate the capabilities of the mission. We will study in future work the possible improvement in the atmospheric characterization if transit and direct-imaging observations are combined.

3.4. Habitable zone planets

One of the main goals of the next generation of space telescopes is to characterize the atmospheres of exoplanets in the habitable zone of their host stars. Although the number of such planets discovered to date is still scarce due to the sensitivity biases of current detection methods, several dozen have been already confirmed.

Here we discuss the known HZ planets within 20 pc detectable with LIFE, as well as those that are also accessible in reflected starlight to HWO. Figure 5 shows all the systems with HZ-planets detectable ($t_{\text{int}} < 100$ h) with LIFE's reference configuration (green circles). We also show in that figure the planets that are accessible to HWO ($P_{\text{access}} > 25\%$), as a representative configuration of future reflected-starlight missions. Table 5 provides the tally of detectable planets for the three configurations of LIFE and HWO. It also shows the total sum of integration time ($\sum t_{\text{int}}$) required for detecting (broadband $S/N = 7$) the LIFE-detectable HZ planets. We consider both the optimistic and conservative HZ as defined by Kopparapu et al. (2014). In all cases, we take as reference the HZ for a $1M_{\oplus}$ planet computed with their Eq. (4).

A total of 38 known HZ planets are detectable with LIFE's reference configuration. For 13 of these planets, we estimate masses lower than $5M_{\oplus}$ (tau Cet e, GJ 667 C c, e and f, Teegarden's Star b and c, Ross 128 b, GJ 273 b, Ross 508 b, Wolf 1061 c, Proxima Centauri b, GJ 3323 b, and GJ 1061 d). We find 8 planets with masses between $5M_{\oplus}$ – $10M_{\oplus}$ (GJ 180 d, GJ 433 d, HIP 38594 b, GJ 682 b, GJ 163 c, GJ 514 b, GJ 357 d, and HD 40307 g). We also find 11 planets with masses between $10M_{\oplus}$ – $1M_{\text{Jup}}$ (HD 69830 d, GJ 422 b, HD 192310 c, GJ 96 b, GJ 1148 b, HD 180617 b, HD 147379 b, 55 Cnc f, GJ 876 c, GJ 687 b, and HD 216520 c). Finally, 6 planets are found with $M_p > 1M_{\text{Jup}}$ (HD 160691 b, 47 UMa b, bet Pic c, HD 10647 b, HD 147513 b, and ups And d). In summary, out of the total 38 LIFE-detectable HZ planets, 34% of them have $M_p < 5M_{\oplus}$, 21% have $5M_{\oplus} < M_p < 10M_{\oplus}$, 29% have $10M_{\oplus} < M_p < 1M_{\text{Jup}}$ and 16% have $M_p > 1M_{\text{Jup}}$.

For comparison, 13 of the HZ-planets within 20 pc are accessible to HWO in reflected starlight. Of these, one has a mass lower than $5M_{\oplus}$ (tau Cet e), two have mass between 5 and $10M_{\oplus}$ (HD 40307 g, GJ 514 b), four have masses between $10M_{\oplus}$ – $1M_{\text{Jup}}$ (HD 69830 d, HD 192310 c, HD 180617 b, and 55 Cnc f), and six have masses larger than $1M_{\text{Jup}}$ (HD 160691 b, 47 UMa b, bet Pic c, HD 10647 b, HD 147513 b, and ups And d). Out of the 13 HWO-accessible HZ planets, 8% have $M_p < 5M_{\oplus}$, 15% have $5M_{\oplus} < M_p < 10M_{\oplus}$, 31% have $10M_{\oplus} < M_p < 1M_{\text{Jup}}$ and 46% have $M_p > 1M_{\text{Jup}}$. This HWO bias happens because the majority of nearby low-mass HZ planets discovered to date orbit M stars at small angular separations.

Some of these HZ planets, in particular those on long-period orbits, might host exomoons potentially detectable through the light modulations produced by mutual transits and shadows (Cabrera & Schneider 2007) or by spectroastrometry (Agol et al. 2015). Dobos et al. (2021) report long-term dynamical stability

Table 5. Detectability of known habitable-zone planets within 20 pc with LIFE and the HWO reflected-starlight notional mission.

	LIFE 4×1 m		LIFE 4×2 m		LIFE 4×3.5 m		HWO
	Tally	$\sum t_{\text{int}}$	Tally	$\sum t_{\text{int}}$	Tally	$\sum t_{\text{int}}$	
Total HZ	32	424	38	138	38	15	13
$< 5M_{\oplus}$	9	94	13	77	13	8	1
$5M_{\oplus}$ – $10M_{\oplus}$	6	212	8	54	8	6	2
$10M_{\oplus}$ – $1M_J$	11	111	11	7	11	0.8	4
$> 1M_J$	6	7	6	0.4	6	0.06	6

Notes. For LIFE, the total sum of integration time needed to detect those planets ($\sum t_{\text{int}}$ [h]) is also indicated.

for a potential exomoon – with survival rates greater than $\sim 40\%$ – for nine of the LIFE-detectable HZ planets. The majority of them are more massive than $1M_{\text{Jup}}$ (HD 160691 b – i.e. mu Arae b –, 47 UMa b, bet Pic c, HD 10647 b, HD 147513 b and ups And d) although some of them have lower masses (HD 40307 g, HD 69830 d, and 55 Cnc f). Given their rather long orbital periods, we find these nine planets to be common targets for LIFE and reflected-starlight telescopes (Table 3). The possible spectral contamination caused by exomoons and the sensitivity required to detect these objects with different instruments will be addressed in future work.

Figure 5 shows that most of the LIFE-detectable HZ planets are part of multi-planet systems. In 20 of these systems, additional planets outside the HZ (both inwards and outwards) are detectable. LIFE will thus be able to probe a significant number of planets in the regions generally considered too hot or too cold to sustain liquid water on the planetary surface. Probing the diversity of planetary atmospheres both within and outside the HZ is a key to understanding the requirements for exoplanets to develop potentially habitable environments.

Planet population statistics predict that there should be hundreds of HZ planets within 20 pc from the Sun, most of which are still undiscovered (e.g. Quanz et al. 2022b). LIFE will be sensitive to most of the newly discovered HZ planets around nearby stars of any spectral type. Reflected-starlight missions might miss those around M stars, but will be sensitive to those orbiting FGK stars. Potential Earth analogues around Sun-like stars will therefore be prime targets for synergistic characterization both in thermal emission and reflected starlight.

4. Discussion

In this work we have adopted several assumptions to consistently process and analyse the complete dataset of known exoplanets. Below we discuss the possible influence of these assumptions on the final results.

– We focused on the population of known exoplanets within 20 pc because these are especially favourable for atmospheric characterization. There is however no strict limit on the distances at which LIFE can detect planets. Indeed, we do not find a decrease in the detectability of low-mass planets as d increases within 0–20 pc (Figs. 1 and C.1). This suggests that 20 pc is a rather conservative limit and extending the analysis further out will increase the target list provided here.

– We assumed a total 5% instrument throughput for all LIFE scenarios, which is a rather conservative value. Given that no instrumental errors are considered as yet, our calculations assume photon-noise limit and the yield scales roughly as the square root of the integration time and thus the square-root of



Fig. 5. Planetary systems with HZ planets detectable with LIFE’s reference configuration. Planets detectable with LIFE are shown by green circles and those which are not, by black circles. Inscribed white-star markers indicate planets that are accessible with HWO in reflected starlight ($P_{\text{access}} > 25\%$). Blue-shaded regions show the conservative HZ of each star, with lighter-blue regions being the optimistic HZ zone (Kopparapu et al. 2014). The sizes of the markers both for stars and planets are proportional to their masses. Stars are color-coded depending on their spectral type (red, orange, yellow, blue-grey and light blue for M, K, G, F and A stars resp.). The Solar System is depicted in the first subplot for reference.

the throughput. Kammerer et al. (2022) found that increasing the throughput to 20% would increase the predicted detection yield by a factor of about two. Such a throughput would reduce the t_{int} presented in this work or, respectively, the mirror size needed to achieve it.

– For all the LIFESim computations shown in this work we assumed an exozodiacal dust level of 3 zodi. To test the effect of other dust levels, we repeated all computations for a value of 27 zodi (the 95% confidence upper limit from the HOSTS survey, Ertel et al. 2020). We found that the number of LIFE-detectable planets does not change for any of the three scenarios considered. We found nevertheless a mean increase of about 40% in the required t_{int} to achieve a detection with LIFE’s reference configuration (resp. an increase of 20% and 60% in t_{int} for LIFE’s pessimistic and optimistic configurations).

– We assumed all planet-hosting stars as single. While wide binaries will not affect the detectability with LIFE dramatically, close binaries will lead to stellar leakage. This is because with nulling interferometry, only the on-axis source can be suppressed (i.e., nulled) while off-axis sources leak through the interferometer. We note that seven of the systems containing LIFE-detectable HZ planets are known to be multiple. These are: GJ 667 C (triple system), HD 147513 (binary), Proxima Cen (triple), HD 180617 (binary), ups And (binary), HD 147379 (binary), and 55 Cnc (binary).

– In our S/N computations for LIFE we did not account for the orbital motion of the planets during the integration time. This might blur the signal of the planet and hinder its characterization, especially for short-period planets with long t_{int} . On the other hand, accounting for the orbital motion of a planet in multi-epoch imaging campaigns has been shown to help increase the S/N of the planet detection (Le Coroller et al. 2022). For LIFE’s reference configuration, we find six planets with t_{int} greater than 10% of the orbital period (GJ 367 b, LHS 1678 c, LHS 1140 c, GJ 3929 b, and TRAPPIST-1 b and c). TRAPPIST-1 b and c have indeed $t_{\text{int}} > P$.

– Similarly, we did not consider the impact of having several planets in the field of view when observing multi-planet systems (see Saxena 2022, for reflected-starlight measurements). Accurate ephemerides of the planets in the system will help in extracting the signal of each point source from LIFE’s interferometric data. We note that RV alone does not provide information on the orbital inclination, and current astrometry facilities such as *Gaia* are generally not sensitive to nearby low-mass planets. This highlights additional synergies of LIFE with HWO and with ground-based direct-imaging instruments – which will provide high-accuracy ephemerides. In multi-planet systems, additional integration time may be required to avoid the signals of each planet being contaminated by that of other planets. We note, however, that only five out of the 212 detectable planets with LIFE’s reference configuration have t_{int} between 50 and 100 h. Given that exozodi shot noise – already included in LIFESim – is expected to dominate over planetary shot noise in the mid-IR, the tally of detectable planets is not expected to be significantly affected. Future work will quantify these effects.

– When computing T_{eq} for each planet (Eq. (1)) we assumed in all cases $A_{\text{B}} = 0.45$ and an efficient heat redistribution consistent with fast-rotating planets ($f = 1$). If a planet is tidally locked, the heat redistribution factor f will be 0.5 and the value of T_{eq} will be higher than reported here.

– By working with T_{eq} , we also assume negligible contribution of internal heat. This effect is especially relevant for young exoplanets, as well as for mature giant ones. It will result in an effective temperature higher than our computed T_{eq} . Such an

increase in the effective temperature will reduce the t_{int} required to detect the planet. This effect will increase the detectability of mature long-period giant exoplanets – to which HWO is particularly sensitive (Fig. B.1) – in the mid-IR with LIFE. The overlap between both missions is thus expected to be higher than reported in this work.

– In Sect. 3.4, we took the habitable zone for a $1M_{\oplus}$ planet as defined in Kopparapu et al. (2014). As shown in their work, for planets with $M_{\text{p}} > 1M_{\oplus}$ the conservative HZ will actually be wider than the one considered here.

– To determine whether a planet is in the HZ or not, we took into account the value of the semi-major axis. Depending on the orbital eccentricity, we note that additional planets to those reported in Sect. 3.4 might enter the HZ during a fraction of their orbit. Also, some of the planets in Sect. 3.4 may leave the HZ during a fraction of their orbit depending on their eccentricity. Analysing these effects on the climate of such planets is out of the scope of this work.

– Our reflected-starlight detectability computations are based only on the angular separation (IWA, OWA) and brightness of the planet (C_{min}), assuming $A_{\text{g}} = 0.3$ and Lambertian scattering. Additional considerations and mission-specific noise models will be needed to determine if a planet reported here as accessible ($P_{\text{access}} > 25\%$) in reflected starlight is actually detectable.

– Our approach based on the known exoplanets is limited by the current detection biases and the accuracy of the orbital characterization of these systems. Both factors are expected to improve in the next years with ongoing transit and RV efforts (e.g. Quirrenbach et al. 2014; Pepe et al. 2021; Lillo-Box et al. 2022), astrometric measurements by *Gaia* (e.g. Reylé et al. 2021) and GRAVITY (Lacour et al. 2020), and preliminary direct-imaging measurements.

– Ground-based ELTs will also directly image known nearby planets (Quanz et al. 2015) and will search for others still unknown (Bowens et al. 2021). ELTs will complement HWO by directly imaging in reflected starlight a number of nearby low-mass exoplanets around M stars (Kasper et al. 2021), a challenging population for HWO due to its smaller mirror size. Combined with HWO, ELTs will thus increase the overlap between reflected-starlight facilities and LIFE. We will further analyse these synergies with ELTs in future work.

– The completeness of our catalogue is limited by the reported parameters in the NASA Exoplanet Archive. Using the Default Parameter Set of the Planetary Systems database ensures self-consistently reported planetary parameters. However, this dataset might lack in some cases parameters that are reported in other references. Also, certain orbital parameters may not be homogeneously reported (see footnote 6).

5. Summary and conclusions

In this work we have shown the potential of a mid-IR space-based nulling interferometer to directly image the thermal emission of the known exoplanets within 20 pc. The scientific theme of detecting and characterizing temperate terrestrial exoplanets in the mid-IR was given very high priority by ESA’s Voyage 2050 Senior Committee report⁸ and is considered a candidate topic for a future L-class mission in the ESA Science Programme. We applied our detectability study to several possible configurations of the Large Interferometer For Exoplanets mission concept. Furthermore, we determined which of these known exoplanets are also accessible with a reflected-starlight mission such as the ~6m Habitable Worlds Observatory highlighted in the

⁸ <https://www.cosmos.esa.int/web/voyage-2050>

US Astro 2020 Decadal Survey recommendations, assuming performance estimates motivated by previous studies.

The mid-IR wavelength range is sensitive to multiple gaseous species – e.g. H₂O, CO₂, CH₄ or O₃ – relevant for habitability analyses of low-mass exoplanets. This spectral range is not particularly sensitive to the aerosols in the atmosphere, but this enables to constrain the planetary radius and the atmospheric temperature-pressure profile eventually down to the surface. On the other hand, the optical and near-IR range will help constrain the properties of the clouds and aerosols in the atmosphere. These wavelengths can also probe phenomena such as the glint of oceans and the vegetation red-edge. However, the sensitivity of the visible spectral region to atmospheric aerosols introduces parameter degeneracies when interpreting reflected-starlight measurements, for instance between the optical properties of the aerosols, those of the surface, the abundance of gaseous species and the value of the planet radius if unknown.

Combining observations in thermal emission and in reflected starlight will yield a much more complete characterization of the planet by breaking the parameter degeneracies and uncertainties of each individual technique. First, multi-wavelength measurements will break the radius-albedo degeneracy, deriving the wavelength-dependent albedo of the planet, which contains key information on the atmospheric composition and cloud structure. The combination of both spectral ranges will allow us to assess the energy budget of the planet and eventually its surface temperature. From that, evidence of atmospheric greenhouse could be inferred if the measured brightness temperature of the planet is higher than its equilibrium temperature. Planets observable with both techniques will be ideal targets for atmospheric characterization.

We find that the reference configuration of LIFE (four 2-m telescopes with a total throughput of 5% and wavelength range between 4–18.5 μm) is able to detect ($S/N = 7$ achieved in less than 100 h) 212 of the total 259 (82%) known exoplanets within 20 pc. In particular, it can detect 144 planets with $M_p < M_{\text{Neptune}}$ (89%) and 68 with $M_p > M_{\text{Neptune}}$ (69%). The notional HWO mission has a similar performance for massive planets, with 64 nearby exoplanets with $M_p > M_{\text{Neptune}}$ accessible ($P_{\text{access}} > 25\%$) in reflected starlight. For currently-known low-mass ($M_p < M_{\text{Neptune}}$) planets, the tally drops to 16 for HWO. This is due to the current observational biases that favour the discovery of low-mass exoplanets around low-mass stars. Their small planet-star angular separations fall inside the IWA of reflected-starlight instruments, and the planets are therefore masked together with the star (see Fig. 1, bottom row). On the other hand, a mid-IR nulling interferometer is very effective at detecting these targets.

A total of 49 exoplanets within 20 pc are detectable with LIFE's reference configuration and are also accessible in reflected starlight with HWO. Most of these common targets are giant planets, although we also find some low-mass ones such as the super-Earths tau Cet e, f and h, HD 20794 d and e, and GJ 514 b. LIFE's reference configuration can also detect 163 exoplanets which are not accessible to HWO (Table D.1). Of these, 62 planets have masses lower than $5M_{\oplus}$, 37 of which require less than 1 h of integration time to be detected with $S/N = 7$. While some overlap already exists between the currently known exoplanets accessible to the assumed LIFE and HWO mission concepts, we expect a much larger overlap between the population of new exoplanets that will be detected by these two missions. That is because the bulk of currently known exoplanets has been detected by RV and transit techniques at small orbital separations.

Of the 40 exoplanets within 20 pc that have been detected in transit to date, LIFE will be able to detect 32. These are generally in the super-Earth to Neptune-like mass range with T_{eq} between 500 and 700 K, but also include planets with $T_{\text{eq}} > 1000$ K. Eight systems have multiple LIFE-detectable transiting planets. We find none of these 40 transiting planets to be accessible with HWO. Transiting planets have and will be intensively monitored by current and future instruments – e.g. CHEOPS, JWST, PLATO, Ariel and ground-based telescopes. Complementary direct-imaging observations could characterize deeper atmospheric layers, although we leave the detailed analysis of multi-technique atmospheric retrievals for future work.

LIFE's reference configuration will detect 38 known exoplanets in the habitable zone of their host star, all of which have been discovered in RV and do not transit. Of these, 13 planets have masses lower than $5M_{\oplus}$ and eight planets have masses between $5M_{\oplus}$ and $10M_{\oplus}$. Even in LIFE's pessimistic configuration with four 1-m telescopes and total 5% throughput, the tally remains nine and six, respectively. We find that HWO can access a lower number of known HZ planets (13, of which three have $M_p < 10M_{\oplus}$) due to the aforementioned observational biases.

The integration time required for LIFE to characterize the atmospheres of these planets will depend on the planet size and temperature, the distance to the planetary system and the stellar type of the host. This will determine the S/N and R needed to constrain the abundance of a given species with a certain level of precision, depending on the science case. Current estimates for LIFE's reference configuration with 5% throughput range from 1 h to detect PH₃ in the atmosphere of a warm giant planet orbiting a G star at 10 pc (Angerhausen et al. 2023) to between 50 and 100 days to detect CH₄ and constrain the abundance of H₂O, CO₂ and O₃ on an Earth twin at 10 pc (Konrad et al. 2022; Alei et al. 2022). Future work will address this in detail for a number of LIFE-detectable planets.

Characterizing the atmospheres of low-mass temperate exoplanets will represent a giant leap in our understanding of exoplanet diversity. We have shown that a mid-IR nulling interferometer such as LIFE will provide ground-breaking measurements for a relevant sample of these worlds, while additionally being able to characterize a wider variety of planets spanning several orders of magnitude in age, mass, and stellar irradiation. LIFE will be able to constrain the planet radius – and hence its density when RV data is available –, the abundance of several potential biomarkers, and the atmospheric T-P profile probing in some cases down to the planet surface. The target list presented here demonstrates the feasibility of these science goals with the exoplanets already known. This list is expected to increase significantly in the coming years as a result of long-baseline transit and RV campaigns, thus increasing the potential for analysing a large population of diverse nearby exoplanets.

Acknowledgements. We thank the anonymous referee for the helpful comments which improved the manuscript. O.C.G. acknowledges the financial support of the API Exoplanètes – Observatoire de Paris. Part of work has been carried out within the framework of the National Centre of Competence in Research PlanetS supported by the Swiss National Science Foundation under grants 51NF40_182901 and 51NF40_205606. D.A., F.D., and S.P.Q. acknowledge the financial support of the SNSF. This research has made use of the NASA Exoplanet Archive, which is operated by the California Institute of Technology, under contract with the National Aeronautics and Space Administration under the Exoplanet Exploration Program.

References

Agol, E., Jansen, T., Lacy, B., Robinson, T. D., & Meadows, V. 2015, *ApJ*, **812**, 5
Akeson, R. L., Chen, X., Ciardi, D., et al. 2013, *PASP*, **125**, 989

- Alei, E., Konrad, B. S., Angerhausen, D., et al. 2022, *A&A*, 665, A106
- Angerhausen, D., Ottiger, M., Dannert, F., et al. 2023, *Astrobiology*, 23, 183
- Anglada-Escudé, G., Arriagada, P., Vogt, S. S., et al. 2012, *ApJ*, 751, A16
- Anglada-Escudé, G., Tuomi, M., Gerlach, E., et al. 2013, *A&A*, 556, A126
- Anglada-Escudé, G., Amado, P. J., Barnes, J., et al. 2016, *Nature*, 536, 437
- Astudillo-Defru, N., Forveille, T., Bonfils, X., et al. 2017, *A&A*, 602, A88
- Baglin, A., Auvergne, M., Barge, P., et al. 2006, *ESA Spec. Publ.*, 1306, 33
- Barstow, J. K., & Irwin, P. G. J. 2016, *MNRAS*, 461, L92
- Beichman, C., Benneke, B., Knutson, H., et al. 2014, *PASP*, 126, 1134
- Bolcar, M. R., Feinberg, L., France, K., et al. 2016, *SPIE Conf. Ser.*, 9904, 99040J
- Bonfils, X., Delfosse, X., Udry, S., et al. 2013, *A&A*, 549, A109
- Bonfils, X., Almenara, J. M., Cloutier, R., et al. 2018a, *A&A*, 618, A142
- Bonfils, X., Astudillo-Defru, N., Díaz, R., et al. 2018b, *A&A*, 613, A25
- Borucki, W. J., Koch, D., Basri, G., et al. 2010, *Science*, 327, 977
- Bourrier, V., Osorio, M. R. Z., Allart, R., et al. 2022, *A&A*, 663, A160
- Bowens, R., Meyer, M. R., Delacroix, C., et al. 2021, *A&A*, 653, A8
- Brown, R. A. 2015, *ApJ*, 805, 188
- Cabrera, J., & Schneider, J. 2007, *A&A*, 464, 1133
- Carrión-González, Ó., García Muñoz, A., Cabrera, J., et al. 2020, *A&A*, 640, A136
- Carrión-González, Ó., García Muñoz, A., Santos, N. C., et al. 2021a, *A&A*, 651, A7
- Carrión-González, Ó., García Muñoz, A., Santos, N. C., et al. 2021b, *A&A*, 655, A92
- Damiano, M., & Hu, R. 2020, *AJ*, 159, 175
- Dannert, F. A., Ottiger, M., Quanz, S. P., et al. 2022, *A&A*, 664, A22
- Defrère, D., Léger, A., Absil, O., et al. 2018, *SPIE Conf. Ser.*, 10701, 107011H
- Dietrich, J., & Apai, D. 2021, *AJ*, 161, 17
- Dobos, V., Charnoz, S., Pál, A., Roque-Bernard, A., & Szabó, G. M. 2021, *PASP*, 133, 094401
- Dong, C., Lingam, M., Ma, Y., & Cohen, O. 2017, *ApJ*, 837, L26
- Dreizler, S., Jeffers, S. V., Rodríguez, E., et al. 2020, *MNRAS*, 493, 536
- Ertel, S., Defrère, D., Hinz, P., et al. 2020, *AJ*, 159, 177
- Feliz, D. L., Blank, D. L., Collins, K. A., et al. 2019, *AJ*, 157, 226
- Feng, F., Tuomi, M., Jones, H. R. A., et al. 2017, *AJ*, 154, 135
- Feng, Y. K., Robinson, T. D., Fortney, J. J., et al. 2018, *AJ*, 155, 200
- Feroz, F., & Hobson, M. P. 2014, *MNRAS*, 437, 3540
- Fitzgerald, M. P., Sallum, S., Millar-Blanchaer, M. A., et al. 2022, *SPIE Conf. Ser.*, 12184, 1218426
- Gaia Collaboration (Brown A. G. A., et al.) 2018, *A&A*, 616, A1
- García Muñoz, A., & Isaak, K. G. 2015, *PNAS*, 112, 13461
- García Muñoz, A., Zapatero Osorio, M. R., Barrera, R., et al. 2012, *ApJ*, 755, 103
- Gardner, J. P., Mather, J. C., Clampin, M., et al. 2006, *Space Sci. Rev.*, 123, 485
- Gardner, J. P., Mather, J. C., Abbott, R., et al. 2023, *PASP*, 135, 068001
- Gaudi, B. S., Seager, S., Mennesson, B., et al. 2018, *ArXiv e-prints* [arXiv:1809.09674]
- Geballe, T. R., Knapp, G. R., Leggett, S. K., et al. 2002, *ApJ*, 564, 466
- Greaves, J. S., Wyatt, M. C., Holland, W. S., & Dent, W. R. F. 2004, *MNRAS*, 351, L54
- Greene, T. P., Bell, T. J., Ducrot, E., et al. 2023, *Nature*, 618, 39
- Hansen, J. T., Ireland, M. J., & LIFE Collaboration. 2022, *A&A*, 664, A52
- Hansen, J. T., Ireland, M. J., Laughier, R., & LIFE Collaboration. 2023, *A&A*, 670, A57
- Harakawa, H., Takarada, T., Kasagi, Y., et al. 2022, *PASJ*, 74, 904
- Hatzes, A. P., & Rauer, H. 2015, *ApJ*, 810, L25
- Herath, M., Gunesequera, S., & Jayaratne, C. 2021, *MNRAS*, 500, 333
- Houllé, M., Vigan, A., Carlotti, A., et al. 2021, *A&A*, 652, A67
- Householder, A., & Weiss, L. 2022, *ArXiv e-prints* [arXiv:2212.06966]
- Howard, W. S., Tilley, M. A., Corbett, H., et al. 2018, *ApJ*, 860, L30
- Howell, S. B., Sobeck, C., Haas, M., et al. 2014, *PASP*, 126, 398
- Hunziker, S., Schmid, H. M., Mouillet, D., et al. 2020, *A&A*, 634, A69
- Jenkins, J. S., Harrington, J., Challener, R. C., et al. 2019, *MNRAS*, 487, 268
- Kammerer, J., & Quanz, S. P. 2018, *A&A*, 609, A4
- Kammerer, J., Quanz, S. P., Dannert, F., & LIFE Collaboration 2022, *A&A*, 668, A52
- Kane, S. R., von Braun, K., Henry, G. W., et al. 2017, *ApJ*, 835, 200
- Kasdin, N. J., Bailey, V. P., Mennesson, B., et al. 2020, *SPIE Conf. Ser.*, 11443, 114431U
- Kasper, M., Cerpa Urra, N., Pathak, P., et al. 2021, *The Messenger*, 182, 38
- Kipping, D. M., Cameron, C., Hartman, J. D., et al. 2017, *AJ*, 153, 93
- Konrad, B. S., Alei, E., Quanz, S. P., et al. 2022, *A&A*, 664, A23
- Kopparapu, R. K., Ramirez, R. M., Schottelkotte, J., et al. 2014, *ApJ*, 787, L29
- Kreidberg, L., & Loeb, A. 2016, *ApJ*, 832, L12
- Lacour, S., Wang, J. J., Nowak, M., et al. 2020, *SPIE Conf. Ser.*, 11446, 1144600
- Lacy, B., & Burrows, A. 2020, *ApJ*, 892, 151
- Lawler, S. M., Di Francesco, J., Kennedy, G. M., et al. 2014, *MNRAS*, 444, 2665
- Lay, O. P. 2004, *Appl. Opt.*, 43, 6100
- Le Coroller, H., Nowak, M., Wagner, K., et al. 2022, *A&A*, 667, A142
- Li, L., Jiang, X., West, R. A., et al. 2018, *Nat. Commun.*, 9, 3709
- Lillo-Box, J., Santos, N. C., Santerne, A., et al. 2022, *A&A*, 667, A102
- Liu, H.-G., Jiang, P., Huang, X., et al. 2018, *AJ*, 155, 12
- López-Morales, M., Triaud, A. H. M. J., Rodler, F., et al. 2014, *ApJ*, 792, L31
- Lovis, C., Snellen, I., Mouillet, D., et al. 2017, *A&A*, 599, A16
- Lupu, R. E., Marley, M. S., Lewis, N., et al. 2016, *AJ*, 152, 217
- Lustig-Yaeger, J., Meadows, V. S., Tovar Mendoza, G., et al. 2018, *AJ*, 156, 301
- MacGregor, M. A., Lawler, S. M., Wilner, D. J., et al. 2016, *ApJ*, 828, 113
- MacGregor, M. A., Weinberger, A. J., Wilner, D. J., Kowalski, A. F., & Cramer, S. R. 2018, *ApJ*, 855, L2
- Males, J. R., Close, L. M., Haffert, S. Y., et al. 2022, *SPIE Conf. Ser.*, 12185, 121854J
- Mamajek, E. E., & Hillenbrand, L. A. 2008, *ApJ*, 687, 1264
- Mawet, D., Fitzgerald, M. P., Konopacky, Q., et al. 2022, *SPIE Conf. Ser.*, 12184, 121841R
- Mennesson, B., Gaudi, S., Seager, S., et al. 2016, *SPIE Conf. Ser.*, 9904, 99040L
- Misra, A., Meadows, V., & Crisp, D. 2014, *ApJ*, 792, 61
- National Academies of Sciences Engineering and Medicine. 2021, *Pathways to Discovery in Astronomy and Astrophysics for the 2020s* (Washington, DC: The National Academies Press)
- Nayak, M., Lupu, R., Marley, M. S., et al. 2017, *PASP*, 129, 034401
- Noack, L., Kislyakova, K. G., Johnstone, C. P., Güdel, M., & Fossati, L. 2021, *A&A*, 651, A103
- Otegi, J. F., Bouchy, F., & Helled, R. 2020, *A&A*, 634, A43
- Pepe, F., Cristiani, S., Rebolo, R., et al. 2021, *A&A*, 645, A96
- Pozuelos, F. J., Suárez, J. C., de Elía, G. C., et al. 2020, *A&A*, 641, A23
- Quanz, S. P., Crossfield, I., Meyer, M. R., Schmalzl, E., & Held, J. 2015, *Int. J. Astrobiol.*, 14, 279
- Quanz, S. P., Kammerer, J., Defrère, D., et al. 2018, *SPIE Conf. Ser.*, 10701, 1070111
- Quanz, S. P., Absil, O., Benz, W., et al. 2022a, *Exp. Astron.*, 54, 1197
- Quanz, S. P., Ottiger, M., Fontanet, E., et al. 2022b, *A&A*, 664, A21
- Quirrenbach, A., Amado, P. J., Caballero, J. A., et al. 2014, *SPIE Conf. Ser.*, 9147, 91471F
- Rauer, H., Gebauer, S., Paris, P. V., et al. 2011, *A&A*, 529, A8
- Rauer, H., Catala, C., Aerts, C., et al. 2014, *Exp. Astron.*, 38, 249
- Reylé, C., Jardine, K., Fouqué, P., et al. 2021, *A&A*, 650, A201
- Ribas, I., Gregg, M. D., Boyajian, T. S., & Bolmont, E. 2017, *A&A*, 603, A58
- Ricker, G. R., Winn, J. N., Vanderspek, R., et al. 2014, *SPIE Conf. Ser.*, 9143, 914320
- Robertson, P., & Mahadevan, S. 2014, *ApJ*, 793, L24
- Sagan, C., Thompson, W. R., Carlson, R., Gurnett, D., & Hord, C. 1993, *Nature*, 365, 715
- Santos, N. C., Sousa, S. G., Mortier, A., et al. 2013, *A&A*, 556, A150
- Saxena, P. 2022, *ApJ*, 934, L32
- Scheucher, M., Herbst, K., Schmidt, V., et al. 2020, *ApJ*, 893, 12
- Schneider, J., Dedieu, C., Le Sidaner, P., Savalle, R., & Zolotukhin, I. 2011, *A&A*, 532, A79
- Schwieterman, E. W., Kiang, N. Y., Parenteau, M. N., et al. 2018, *Astrobiology*, 18, 663
- Seager, S., Turner, E. L., Schafer, J., & Ford, E. B. 2005, *Astrobiology*, 5, 372
- Snellen, I. A. G., Désert, J. M., Waters, L. B. F. M., et al. 2017, *AJ*, 154, 77
- Sousa, S. G., Adibekyan, V., Delgado-Mena, E., et al. 2021, *A&A*, 656, A53
- Souto, D., Unterborn, C. T., Smith, V. V., et al. 2018, *ApJ*, 860, L15
- Spergel, D., Gehrels, N., Baltay, C., et al. 2015, *ArXiv e-prints* [arXiv:1503.03757]
- Stassun, K. G., Oelkers, R. J., Paegert, M., et al. 2019, *AJ*, 158, 138
- Takeda, G., Ford, E. B., Sills, A., et al. 2007, *ApJS*, 168, 297
- The LUVVOIR Team 2018, *ArXiv e-prints* [arXiv:1809.09668]
- Tinetti, G., Drossart, P., Eccleston, P., et al. 2018, *Exp. Astron.*, 46, 135
- Traub, W. A., & Oppenheimer, B. R. 2010, *Direct Imaging of Exoplanets* (University of Arizona Press), 111
- Vida, K., Oláh, K., Kővári, Z., et al. 2019, *ApJ*, 884, 160
- Wandel, A., & Tal-Or, L. 2019, *ApJ*, 880, L21
- Williams, D. M., & Gaidos, E. 2008, *Icarus*, 195, 927
- Wright, D. J., Wittenmyer, R. A., Tinney, C. G., Bentley, J. S., & Zhao, J. 2016, *ApJ*, 817, L20
- Wunderlich, F., Godolt, M., Grenfell, J. L., et al. 2019, *A&A*, 624, A49
- Wunderlich, F., Scheucher, M., Grenfell, J. L., et al. 2021, *A&A*, 647, A48
- Wytenbach, A., Ehrenreich, D., Lovis, C., Udry, S., & Pepe, F. 2015, *A&A*, 577, A62
- Ygouf, M., Zimmerman, N. T., Pueyo, L., et al. 2016, *SPIE Conf. Ser.*, 9904, 99045M
- Zechmeister, M., Dreizler, S., Ribas, I., et al. 2019, *A&A*, 627, A49

Appendix A: Accessible exoplanets in reflected-starlight beyond 20 pc

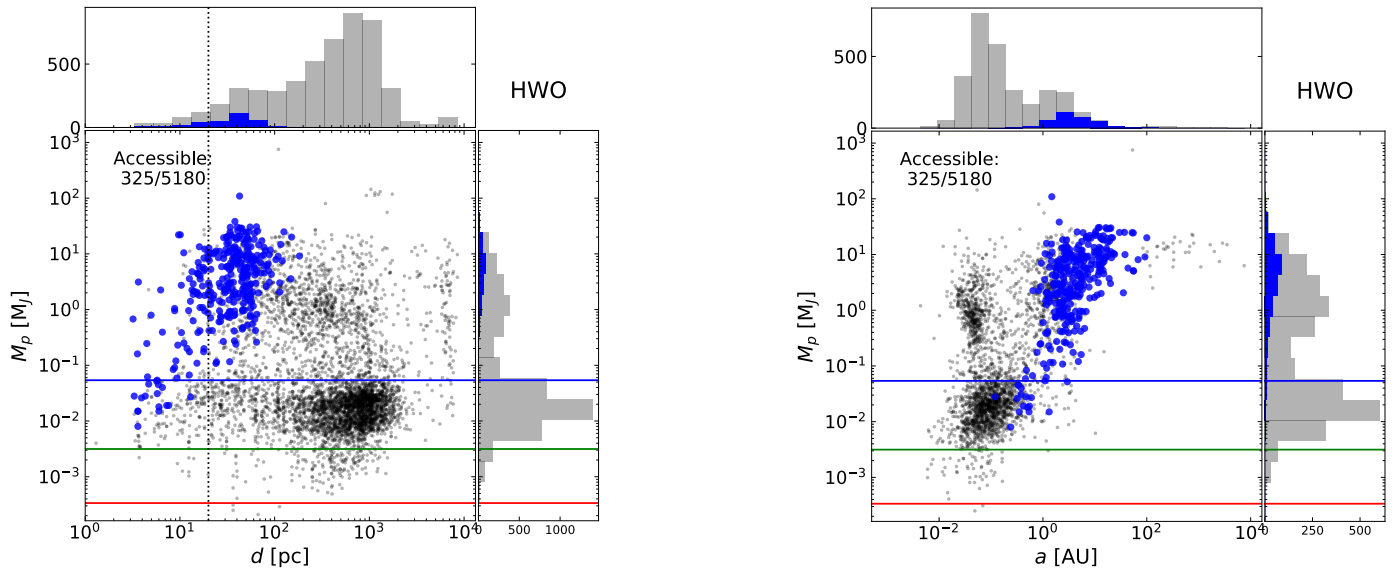


Fig. A.1. As Fig. 1, but including the exoplanets beyond 20 pc with $P_{\text{access}} > 25\%$ for the notional HWO mission. The vertical dotted line indicates the 20 pc threshold.

Appendix B: Exoplanets only accessible with the notional HWO

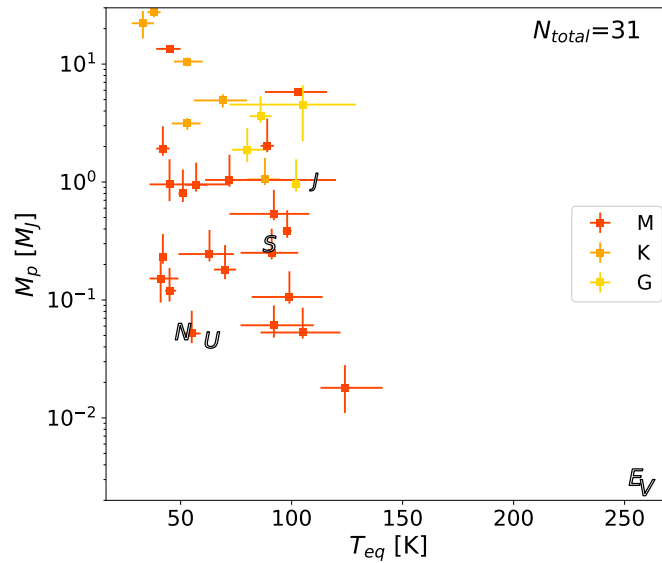


Fig. B.1. As Fig. 4, but for those planets accessible in reflected starlight with the notional HWO and not with LIFE’s reference configuration. These are: GJ 667 C g, HD 115404 A c, GJ 433 c, HD 113538 c, 47 UMa d, HD 153557 d, GJ 317 b, GJ 317 c, GJ 676 A c, GJ 676 A b, GJ 163 d, HIP 38594 c, GJ 229 b, HD 140901 c, HD 145675 c, GJ 3512 c, GJ 3512 b, 55 Cnc d, GJ 687 c, GJ 179 b, GJ 832 b, GJ 9066 c, GJ 680 b, GJ 15 A c, GJ 849 c, HD 95735 c, GJ 1148 c, GJ 849 b, eps Ind A b, TYC 2187-512-1 b, HD 154345 b.

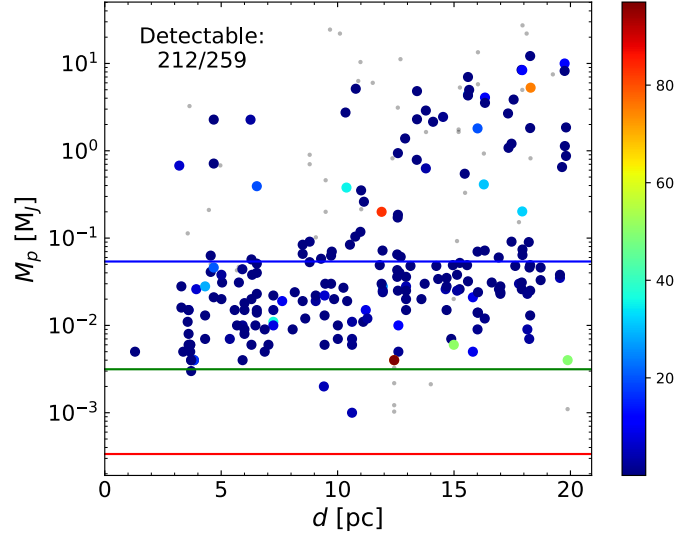
Appendix C: Integration time of the LIFE-detectable exoplanets.


Fig. C.1. LIFE-detectable exoplanets, as in Fig. 1, but colour-coding each planet according to the integration time (in hours) required to be detected with LIFE’s reference configuration.

Appendix D: List of planets only detectable by LIFE

Table D.1. Detectability of the exoplanets within 20 pc that are not accessible in reflected starlight with the notional HWO but can be detected ($S/N = 7$) with LIFE. Integration times longer than 100 h are not considered as detectable and are not shown in the table.

Planet	d [pc]	a [AU]	R_p [R_\oplus]	M_p [M_\oplus]	T_{eq} [K]	LIFE (4x1m)		LIFE (4 × 2 m)		LIFE (4 × 3.5m)	
						S/N (10h)	t_{int} [h]	S/N (10h)	t_{int} [h]	S/N (10h)	t_{int} [h]
GJ 367 b	9.41	0.01	0.67	0.64	1178	3	63	10	5	22	1
L 98-59 b	10.62	0.02	0.90	0.32	534	3	51	10	4	21	1
HD 21749 c	16.32	0.07	0.90	3.81	661	9	6	24	0.8	47	0.2
LHS 1678 c	19.88	0.03	1.01	1.27	468	–	–	3	50	7	10
YZ Cet b	3.71	0.02	1.01	0.95	410	37	0.4	104	0.04	225	0.01
Teegarden’s Star c	3.83	0.04	1.12	1.27	191	–	–	5	17	17	2
Teegarden’s Star b	3.83	0.03	1.12	1.27	253	6	15	21	1	59	0.1
GJ 273 c	5.92	0.04	1.12	1.27	401	20	1	56	0.2	123	0.03
GJ 1132 b	12.61	0.02	1.12	1.59	516	3	42	17	2	37	0.4
GJ 3929 b	15.81	0.03	1.12	1.59	501	–	–	7	9	15	2
LTT 1445 A c	6.87	0.03	1.12	1.59	452	20	1	56	0.2	119	0.03
LHS 1140 c	14.99	0.03	1.12	1.91	357	–	–	3	51	8	8
YZ Cet d	3.71	0.03	1.12	1.27	311	18	1	59	0.1	144	0.02
YZ Cet c	3.71	0.02	1.12	1.27	357	22	1	64	0.1	142	0.02
TRAPPIST-1 c	12.43	0.016	1.12	1.27	323	–	–	3	73	7	10
TRAPPIST-1 b	12.43	0.011	1.12	1.27	379	–	–	2	97	6	15
Ross 128 b	3.37	0.05	1.23	1.59	267	13	3	47	0.2	128	0.03
GJ 581 e	6.30	0.03	1.23	1.91	485	23	0.9	60	0.1	121	0.03
GJ 393 b	7.03	0.05	1.23	1.91	458	26	0.7	72	0.09	156	0.02
Proxima Cen b	1.30	0.05	1.23	1.59	229	45	0.2	170	0.02	466	0.002
LHS 1478 b	18.23	0.02	1.23	2.22	566	–	–	14	2	31	0.5
GJ 357 b	9.44	0.04	1.23	1.91	494	24	0.9	69	0.1	145	0.02
GJ 1061 b	3.67	0.02	1.23	1.59	355	38	0.3	113	0.04	257	0.007
GJ 1061 d	3.67	0.05	1.23	1.91	248	9	6	38	0.3	111	0.04
HD 260655 b	10.01	0.03	1.23	2.22	612	12	3	36	0.4	69	0.1
HD 219134 f	6.53	0.15	1.35	7.31	455	19	1	52	0.2	109	0.04
tau Cet g	3.60	0.13	1.35	1.91	553	56	0.2	134	0.03	261	0.007
LHS 3844 b	14.88	0.01	1.35	2.22	763	4	26	43	0.3	95	0.05
Wolf 1061 b	4.31	0.04	1.35	2.22	404	46	0.2	129	0.03	280	0.006
LTT 1445 A b	6.87	0.04	1.35	2.86	371	15	2	45	0.2	101	0.05
GJ 486 b	8.07	0.02	1.35	2.86	606	18	1	55	0.2	107	0.04
L 98-59 c	10.62	0.03	1.35	2.22	451	6	14	19	1	40	0.3
HD 20794 c	6.00	0.20	1.35	2.54	477	22	1.0	57	0.1	115	0.04
GJ 3323 b	5.37	0.03	1.35	2.22	255	4	29	16	2	43	0.3
GJ 1061 c	3.67	0.03	1.35	1.91	274	15	2	49	0.2	124	0.03

Table D.1. continued.

Planet	d [pc]	a [AU]	R_p [R_\oplus]	M_p [M_\oplus]	T_{eq} [K]	LIFE (4x1m)		LIFE (4x2m)		LIFE (4x3.5m)	
						S/N (10h)	t_{int} [h]	S/N (10h)	t_{int} [h]	S/N (10h)	t_{int} [h]
HD 219134 c	6.53	0.07	1.46	4.45	676	53	0.2	120	0.03	224	0.01
GJ 667 C e	7.24	0.21	1.46	3.50	197	–	–	4	36	11	4
GJ 667 C f	7.24	0.15	1.46	3.18	230	–	–	8	8	22	1.0
GJ 273 b	5.92	0.09	1.46	3.18	251	5	23	18	2	51	0.2
GJ 1132 c	12.61	0.05	1.46	3.18	296	–	–	6	12	17	2
GJ 625 b	6.47	0.08	1.46	3.18	292	9	6	33	0.4	87	0.06
G 264-012 b	16.01	0.02	1.46	2.86	552	4	26	21	1	43	0.3
HD 20794 b	6.00	0.12	1.46	2.86	619	35	0.4	85	0.07	165	0.02
GJ 3998 b	18.15	0.03	1.46	2.86	637	3	45	12	3	25	0.8
GJ 411 b	5.68	0.08	1.46	3.18	335	17	2	56	0.2	135	0.03
HD 219134 d	6.53	0.24	1.57	16.21	357	16	2	48	0.2	109	0.04
HD 219134 b	6.53	0.04	1.57	4.77	876	67	0.1	154	0.02	278	0.006
GJ 740 b	11.10	0.03	1.57	3.50	730	25	0.8	70	0.1	132	0.03
L 98-59 e	10.62	0.07	1.57	3.50	294	4	35	13	3	34	0.4
L 98-59 d	10.62	0.05	1.57	1.91	356	7	11	21	1	50	0.2
HD 260655 c	10.01	0.05	1.57	3.18	481	19	1	51	0.2	105	0.04
GJ 15 A b	3.56	0.07	1.68	3.50	347	49	0.2	148	0.02	339	0.004
CD Cet b	8.61	0.02	1.68	3.81	434	20	1	79	0.08	175	0.02
HD 136352 b	14.68	0.10	1.68	4.77	780	27	0.7	65	0.1	121	0.03
HD 85512 b	11.28	0.26	1.68	3.81	296	4	35	13	3	35	0.4
pi Men c	18.27	0.07	1.79	4.13	1048	22	1	61	0.1	115	0.04
Wolf 1061 c	4.31	0.09	1.79	4.13	261	14	2	53	0.2	145	0.02
GJ 357 c	9.44	0.06	1.79	4.13	378	22	1	69	0.1	165	0.02
GJ 667 C c	7.24	0.12	1.91	4.77	256	5	17	20	1	57	0.1
Ross 508 b	11.21	0.05	1.91	4.77	266	–	–	7	9	21	1
GJ 251 b	5.58	0.08	1.91	4.77	302	19	1	65	0.1	162	0.02
G 264-012 c	16.01	0.05	1.91	4.45	358	5	23	18	2	43	0.3
GJ 676 A d	16.03	0.04	1.91	4.45	689	15	2	44	0.3	85	0.07
55 Cnc e	12.59	0.02	1.91	7.95	1678	21	1	75	0.09	172	0.02
GJ 887 b	3.29	0.07	2.02	5.09	404	97	0.05	265	0.007	560	0.002
HD 40307 b	12.94	0.05	2.02	4.77	818	56	0.2	150	0.02	278	0.006
GJ 433 d	9.06	0.18	2.24	6.04	234	3	41	14	3	41	0.3
GJ 682 b	5.01	0.08	2.24	6.36	238	12	4	45	0.2	124	0.03
61 Vir b	8.50	0.05	2.24	6.04	1017	108	0.04	257	0.007	463	0.002
HD 40307 f	12.94	0.25	2.24	6.36	354	10	5	35	0.4	87	0.07
GJ 581 c	6.30	0.07	2.35	6.36	302	25	0.8	81	0.07	200	0.01
Gl 49 b	9.85	0.09	2.35	6.36	402	37	0.4	110	0.04	250	0.008
HD 22496 b	13.60	0.05	2.35	6.36	729	84	0.07	221	0.01	419	0.003
GJ 876 d	4.68	0.02	2.35	6.67	531	159	0.02	403	0.003	777	0.0008
GJ 536 b	10.41	0.07	2.35	6.04	420	29	0.6	81	0.07	173	0.02
GJ 667 C b	7.24	0.05	2.47	6.99	406	56	0.2	153	0.02	327	0.005
GJ 433 b	9.06	0.06	2.47	6.99	408	34	0.4	93	0.06	197	0.01
GJ 3929 c	15.81	0.08	2.47	6.67	279	–	–	7	9	20	1
GJ 357 d	9.44	0.20	2.47	6.99	205	–	–	9	6	28	0.6
GJ 180 c	11.94	0.12	2.58	7.95	257	5	24	17	2	47	0.2
GJ 143 b	16.32	0.19	2.58	22.88	372	13	3	42	0.3	100	0.05
HD 7924 b	16.99	0.06	2.58	7.31	769	43	0.3	121	0.03	227	0.009
HD 136352 d	14.68	0.43	2.58	8.90	372	11	4	34	0.4	81	0.07
GJ 3998 c	18.15	0.09	2.58	7.31	362	7	11	22	1	52	0.2
GJ 180 b	11.94	0.09	2.69	7.63	296	8	7	27	0.7	69	0.1
Gl 686 b	8.16	0.09	2.69	7.63	330	31	0.5	99	0.05	236	0.009
HD 7924 d	16.99	0.15	2.69	7.63	482	32	0.5	90	0.06	194	0.01
HD 154088 b	18.27	0.13	2.69	7.95	633	51	0.2	133	0.03	267	0.007
HD 40307 c	12.94	0.08	2.69	7.95	620	73	0.09	181	0.01	346	0.004
GJ 676 A e	16.03	0.18	2.69	7.63	320	8	9	26	0.7	66	0.1
GJ 163 c	15.13	0.13	2.69	7.95	264	4	40	13	3	36	0.4
GJ 1214 b	14.64	0.01	2.69	8.26	508	–	–	12	4	25	0.8
GJ 3942 b	16.93	0.06	2.80	8.26	514	21	1	61	0.1	122	0.03
GJ 1265 b	10.25	0.03	2.80	8.58	364	12	4	46	0.2	109	0.04
HD 189567 c	17.91	0.20	2.80	8.26	552	36	0.4	97	0.05	202	0.01
HD 238090 b	15.24	0.09	2.80	8.26	420	24	0.9	69	0.1	151	0.02
GJ 180 d	11.94	0.31	2.91	8.90	184	–	–	4	26	14	2
AU Mic c	9.72	0.11	2.91	9.53	444	51	0.2	154	0.02	353	0.004
HD 7924 c	16.99	0.11	2.91	8.90	555	49	0.2	127	0.03	252	0.008

Table D.1. continued.

Planet	d [pc]	a [AU]	R_p [R_\oplus]	M_p [M_\oplus]	T_{eq} [K]	LIFE (4x1m)		LIFE (4 x 2 m)		LIFE (4 x 3.5m)	
						S/N (10h)	t_{int} [h]	S/N (10h)	t_{int} [h]	S/N (10h)	t_{int} [h]
GJ 414 A b	11.89	0.23	2.91	9.53	319	12	3	44	0.3	114	0.04
HD 136352 c	14.68	0.17	2.91	11.12	584	52	0.2	132	0.03	263	0.007
HD 160691 d	15.60	0.09	3.03	10.17	995	123	0.03	286	0.006	524	0.002
HIP 38594 b	17.79	0.26	3.03	9.53	270	4	36	14	2	41	0.3
HD 285968 b	9.47	0.07	3.03	9.53	415	56	0.2	155	0.02	331	0.004
GJ 3779 b	13.74	0.03	3.03	9.53	454	15	2	59	0.1	127	0.03
GJ 3082 b	16.62	0.08	3.03	9.85	405	19	1	60	0.1	134	0.03
HD 26965 b	5.04	0.22	3.14	9.85	419	120	0.03	323	0.005	670	0.001
HD 189567 b	17.91	0.11	3.14	9.85	741	83	0.07	204	0.01	383	0.003
HIP 54373 b	18.72	0.06	3.14	10.49	509	20	1	62	0.1	126	0.03
GJ 685 b	14.32	0.13	3.25	10.81	317	13	3	44	0.3	107	0.04
HD 216520 c	19.55	0.53	3.25	11.12	256	3	65	11	4	31	0.5
GJ 682 c	5.01	0.19	3.36	12.08	161	3	53	14	3	46	0.2
HD 40307 d	12.94	0.13	3.36	11.44	482	72	0.09	197	0.01	413	0.003
HD 69830 b	12.56	0.08	3.47	11.44	757	159	0.02	379	0.003	702	0.001
HD 216520 b	19.55	0.20	3.47	12.08	417	27	0.7	82	0.07	186	0.01
GJ 338 B b	6.33	0.14	3.59	12.08	339	72	0.09	230	0.009	546	0.002
GJ 163 b	15.13	0.06	3.59	12.08	379	17	2	54	0.2	123	0.03
GJ 422 b	12.66	0.11	3.70	12.71	253	7	10	26	0.7	71	0.1
GJ 674 b	4.55	0.04	3.70	13.03	464	429	0.003	1093	0.0004	2195	0.0001
HD 69830 c	12.56	0.19	3.81	13.67	493	73	0.09	209	0.01	454	0.002
GJ 3222 b	18.24	0.09	3.81	14.62	1671	340	0.004	1180	0.0003	2441	8e-05
HD 211970 b	13.13	0.14	4.04	15.26	348	36	0.4	114	0.04	271	0.007
LSPM J21+02 b ^(a)	17.63	0.09	4.04	15.26	325	12	3	41	0.3	102	0.05
HIP 54373 c	18.72	0.10	4.04	14.62	407	29	0.6	88	0.06	197	0.01
GJ 436 b	9.75	0.03	4.15	22.25	598	152	0.02	419	0.003	804	0.0008
GJ 480 b	14.24	0.07	4.15	15.26	367	27	0.7	85	0.07	193	0.01
HD 141004 b	11.81	0.12	4.15	15.57	828	186	0.01	420	0.003	778	0.0008
GJ 720 A b	15.56	0.12	4.15	15.57	347	27	0.7	83	0.07	196	0.01
pi Men d	18.27	0.50	4.15	15.57	393	25	0.8	77	0.08	178	0.02
Gl 378 b	14.95	0.04	4.15	15.57	611	72	0.09	215	0.01	418	0.003
HD 192310 b	8.80	0.32	4.26	16.84	355	61	0.1	193	0.01	454	0.002
HD 140901 b	15.25	0.08	4.37	16.53	867	197	0.01	511	0.002	941	0.0006
HD 177565 b	16.92	0.25	4.48	19.07	467	54	0.2	161	0.02	364	0.004
GJ 581 b	6.30	0.04	4.60	18.12	402	211	0.01	567	0.002	1181	0.0003
AU Mic b	9.72	0.06	4.71	20.02	500	141	0.02	347	0.004	676	0.001
HD 190007 b	12.71	0.09	4.71	19.39	565	166	0.02	411	0.003	798	0.0008
HD 153557 c	17.94	0.11	4.93	20.34	608	207	0.01	545	0.002	1088	0.0004
GJ 687 b	4.55	0.16	4.93	20.02	231	63	0.1	239	0.009	645	0.001
61 Vir c	8.50	0.22	5.04	20.98	491	198	0.01	540	0.002	1131	0.0004
HD 190360 c	16.01	0.13	5.16	22.25	713	225	0.01	536	0.002	1018	0.0005
GJ 96 b	11.93	0.29	5.27	22.88	245	14	2	57	0.2	168	0.02
HD 153557 b	17.94	0.07	5.38	23.52	669	149	0.02	413	0.003	784	0.0008
HIP 48714 b	10.53	0.11	5.72	26.70	444	229	0.009	682	0.001	1524	0.0002
HD 99492 b	18.21	0.12	5.72	28.60	540	158	0.02	419	0.003	852	0.0007
rho CrB c	17.47	0.41	6.16	28.92	425	65	0.1	192	0.01	427	0.003
HD 147379 b	10.76	0.32	6.73	33.05	242	28	0.6	110	0.04	308	0.005
HD 115404 A b	10.98	0.09	7.17	37.50	618	645	0.001	1547	0.0002	2945	6e-05
55 Cnc c	12.59	0.24	9.64	58.80	428	270	0.007	795	0.0008	1763	0.0002
70 Vir b	17.90	0.48	11.99	2683.64	493	307	0.005	852	0.0007	1794	0.0001
HD 3651 b	11.13	0.29	12.11	82.95	487	858	0.0007	2362	9e-05	4912	2e-05
tau Boo b	15.65	0.05	12.33	1582.73	1454	937	0.0006	2922	6e-05	5933	1e-05
GJ 86 b	10.78	0.11	12.33	1631.35	570	1491	0.0002	3507	4e-05	6617	1e-05
GJ 3021 b	17.56	0.49	12.44	1226.77	362	198	0.01	646	0.001	1532	0.0002
HD 189733 b	19.76	0.03	12.67	360.09	1035	369	0.004	1331	0.0003	2756	6e-05
HIP 79431 b	14.53	0.36	12.78	776.11	156	4	30	19	1	63	0.1
GJ 876 b	4.68	0.21	12.89	723.35	164	54	0.2	241	0.008	761	0.0008
rho CrB b	17.47	0.22	13.23	383.29	582	676	0.001	1653	0.0002	3199	5e-05
55 Cnc b	12.59	0.11	13.34	298.75	619	1363	0.0003	3176	5e-05	5937	1e-05
ups And b	13.40	0.06	13.45	250.44	1313	1481	0.0002	4038	3e-05	7558	1e-05
HD 192263 b	19.64	0.15	13.67	206.90	459	471	0.002	1263	0.0003	2567	7e-05
GJ 876 c	4.68	0.13	13.67	226.92	215	277	0.006	1061	0.0004	2816	6e-05
51 Peg b	15.46	0.05	13.79	173.53	1139	1096	0.0004	3257	5e-05	6332	1e-05
GJ 1148 b	11.01	0.17	14.01	111.87	217	67	0.1	271	0.007	790	0.0008

^(a)LSPM J2116+0234 b

Appendix E: Science cases of low-mass ($M_p < 5M_\oplus$) habitable-zone planets detectable by LIFE

Proxima Cen b: Located in the conservative HZ of our closest stellar neighbour, it has a minimum mass of $1.27M_\oplus$ and an eccentricity $e < 0.35$ (Anglada-Escudé et al. 2016). The M5.5V star has shown high activity levels, with XUV irradiance 60 times that of the Earth (Ribas et al. 2017) and frequent flaring events (MacGregor et al. 2018; Howard et al. 2018; Vida et al. 2019). This stellar activity will affect the habitability conditions of Proxima b (Scheucher et al. 2020) and might lead to atmospheric erosion depending on the planetary magnetic field (Dong et al. 2017). Although potential transits have been reported (Kipping et al. 2017; Liu et al. 2018), no robust evidence has been found as these photometric variations can be caused by stellar activity (Feliz et al. 2019; Jenkins et al. 2019).

Lovis et al. (2017) found that Proxima Cen b could be detected in 20–40 nights of telescope time by coupling upgraded versions of ESPRESSO and SPHERE, with a detection of atmospheric O_2 achievable in 60 nights spread over 3 years. JWST’s MIRI has been proposed to detect the eventual atmosphere of the planet either by measuring thermal phase curves (Kreidberg & Loeb 2016) or through cross-correlation (Snellen et al. 2017). The unknown planet-to-star ratio, the stellar activity and the lack of a measurement of the orbital inclination could however prevent the interpretation of these observations. We find that only LIFE ($S/N=170$ in 10 h of integration time) will be able to directly image Proxima Cen b (Table 3). LIFE will probe the atmospheric components of the planet (Defrère et al. 2018) and its T-P profile, but also its mass and radius. This is key to understand the possible history of the planet, including geological processes such as outgassing which shape the evolution of the atmosphere (Noack et al. 2021).

Ross 128 b: This $1.5M_\oplus$ planet orbits at the inner edge of the optimistic HZ of one of the closest ($d=3.3$ pc) known planetary systems (Bonfils et al. 2018b). The M4 host star shows weak magnetic activity and K2 light curves yielded no transits of the planet (Bonfils et al. 2018a). Based on the stellar properties, Souto et al. (2018) and Herath et al. (2021) suggested a rocky composition with an iron core proportionally larger than that of the Earth.

tau Cet e: A planetary system of four super-Earths with minimum masses between $1.7\text{--}3.9M_\oplus$ was detected in RV around this Sun-like (G8.5V) star (Feng et al. 2017). The age of the system shown in Fig. 5 corresponds to the lower limit reported in the Composite database in the NASA Archive from Takeda et al. (2007), but we also note that Mamajek & Hillenbrand (2008) estimate an age of 5.8 Gyr for this star. We find a mass of about $4.8M_\oplus$ for tau Cet e, which orbits in the inner region of the optimistic HZ with $e \sim 0.2$. Planet f, with similar mass, also orbits near –but slightly outside– the outer boundary of the HZ. Planets e and f are detectable with LIFE and also accessible to HWO in reflected starlight (Table 3). If additional planets are present in the HZ (Dietrich & Apai 2021), they will fall within the detectability region as well. The presence of a debris-disk (Greaves et al. 2004; Lawler et al. 2014) with an inner edge at around 6 AU (MacGregor et al. 2016; Hunziker et al. 2020) might affect the detectability of the planets depending on its inclination and exozodi abundance.

GJ 1061 d: This rather inactive M5.5V star hosts three rocky planets (b, c, d) with minimum masses of 1.37, 1.74 and

$1.64M_\oplus$ (Dreizler et al. 2020). Planet d orbits within the conservative HZ. Planet c, with $T_{eq}=274$ K, orbits close to the inner edge of the optimistic HZ. Upper limits of 0.29 and 0.53 were found for the eccentricity of planets c and d. Follow-up observations will help determine whether GJ 1061 d is one of the few highly eccentric HZ rocky planets known to date and the potential implications for its climate.

GJ 273 b: Astudillo-Defru et al. (2017) found two planet signals (GJ 273 b and c) in HARPS RV data, with two additional candidates in the sub-Neptune regime. Based on dynamical studies, Pozuelos et al. (2020) found a mass of $2.89M_\oplus < M_p < 3.03M_\oplus$ for planet b. We find a slightly higher $M_p=3.2M_\oplus$ and $T_{eq}=251$ K. Planet c, with $M_p \sim 1.3M_\oplus$, $T_{eq}=400$ K and also detectable by LIFE, is an interesting case study on the effect of stellar irradiation on rocky planets.

Teegarden’s Star b and c: To date, these planets are among the most similar to Earth in terms of mass, with $M_p \sin i \sim 1.1M_\oplus$ (Zechmeister et al. 2019) and true masses that we estimate to be $\sim 1.27M_\oplus$. They have almost circular orbits with periods of 4.9 and 11.4 days, and are likely tidally locked. The M7.0V star shows currently low activity (Zechmeister et al. 2019). Wandell & Tal-Or (2019) found that these planets are likely to sustain liquid water –at least on part of their surface– for a wide range of atmospheric configurations. With no transits detected to date, LIFE will be the only mission able to probe the atmospheres of these targets.

Wolf 1061 c: The three planets in the system were detected in RV (Wright et al. 2016; Astudillo-Defru et al. 2017), with planet c being the only HZ one. We obtain for this planet a mass of about $4.1M_\oplus$ and $T_{eq}=261$ K. Wright et al. (2016) estimated a transit probability for planet c of 5.9%, but Kane et al. (2017) detected no transits in 7 years of ground-based photometry. LIFE will be capable of directly imaging this planet (Table D.1) and will also detect planets b and d.

GJ 3323 b: This system hosts two super-Earths with $M_p \sim 2.3M_\oplus$ (Astudillo-Defru et al. 2017), and we find GJ 3323 b (with $T_{eq}=255$ K) to orbit at the inner edge of the optimistic HZ.⁹ Only LIFE will be able to detect this planet, although the outer companion GJ 3323 c will remain out of reach because its $T_{eq}=130$ K will make it much fainter in the mid-IR.

GJ 667 C c, e and f: GJ 667 C is an M1.5V star (Geballe et al. 2002) orbiting the pair of K stars GJ 667 AB at a distance of about 230 AU (e.g. Anglada-Escudé et al. 2013). Planets b and c were the first detected in RV (Bonfils et al. 2013), with additional reported signals for up to five more planets (named b–h) (Anglada-Escudé et al. 2012, 2013). Subsequent reanalyses of the RV data confirmed planets b and c and found no evidence for the other planets (Feroz & Hobson 2014; Robertson & Mahadevan 2014). Currently the NASA Exoplanet Archive includes only planets b, c, e, f, and g, with the latter three marked as controversial. All the planets in the system have low eccentricities, and in particular planets c, e and f have all values around $e=0.1$. Only LIFE will be able to directly image the potential HZ planets in this system.

Ross 508 b: This super-Earth orbits an M4.5 star located at 11 pc. Its orbit has a period of 10.7 days and a rather high eccentricity of 0.33 (Harakawa et al. 2022). We estimate for Ross 508 b a mass of $4.8M_\oplus$ and $T_{eq}=266$ K, placing it at the inner edge of the optimistic HZ. Harakawa et al. (2022) found a transit probability of 1.6% for this planet.

⁹ Astudillo-Defru et al. (2017) reported that planet c was the one in the HZ. We confirmed that this was due to an error in their Table 4 (Astudillo-Defru priv. comm.).

Appendix F: Young planetary systems

Table F.1. Detectability with LIFE of the known exoplanets that have been directly imaged up to date, as reported in the NASA Exoplanet Archive.

Planet	d [pc]	a [AU]	M_p [M_J]	R_p [R_J]	LIFE (4x1m)		LIFE (4 × 2 m)		LIFE (4 × 3.5m)	
					S/N (10h)	t_{int} [h]	S/N (10h)	t_{int} [h]	S/N (10h)	t_{int} [h]
bet Pic b	19.75 ^{+0.09} _{-0.01}	11.30 ^{+2.10} _{-1.74}		1.36 ^{+0.01} _{-0.01}	5498.9	2.0×10 ⁻⁵	16024.0	0.0	33308.8	0.0
HN Peg b	18.12 ^{+0.01} _{-0.01}	773.32 ^{+8.57} _{-8.90}	21.96 ^{+6.513} _{-6.305}	1.09 ^{+0.02} _{-0.07}	3029.8	5.0×10 ⁻⁵	8892.8	1.0×10 ⁻⁵	17268.8	0.0
2MASS J02-39 b ^(a)	39.40 ^{+0.00} _{-0.00}	156.37 ^{+6.30} _{-7.34}	13.853 ^{+0.790} _{-0.751}	1.44 ^{+0.02} _{-0.02}	2677.0	7.0×10 ⁻⁵	8593.5	1.0×10 ⁻⁵	18913.1	0.0
HD 100546 b	109.69 ^{+0.42} _{-0.44}	52.96 ^{+1.41} _{-1.28}		6.71 ^{+1.96} _{-1.76}	2521.6	8.0×10 ⁻⁵	7369.5	1.0×10 ⁻⁵	14678.0	0.0
2MASS J21+16 b ^(b)	33.10 ^{+0.00} _{-0.00}	3.95 ^{+0.47} _{-0.57}	52.666 ^{+35.262} _{-30.226}	0.94 ^{+0.24} _{-0.23}	2430.8	8.0×10 ⁻⁵	7986.9	1.0×10 ⁻⁵	17716.8	0.0
Ross 458 c	11.51 ^{+0.01} _{-0.01}	1100.00 ^{+0.00} _{-0.00}	6.000 ^{+0.000} _{-0.000}	1.07 ^{+0.04} _{-0.05}	2372.3	9.0×10 ⁻⁵	6108.8	1.0×10 ⁻⁵	11774.5	0.0
TYC 8998-760-1 b	94.62 ^{+0.20} _{-0.18}	162.00 ^{+0.00} _{-0.00}	13.900 ^{+2.109} _{-2.014}	2.73 ^{+0.32} _{-0.31}	2041.2	1.2×10 ⁻⁴	6869.9	1.0×10 ⁻⁵	14867.4	0.0
AB Pic b	50.05 ^{+0.05} _{-0.05}	260.00 ^{+0.00} _{-0.00}	13.482 ^{+0.351} _{-0.344}	1.26 ^{+0.17} _{-0.16}	1962.4	1.3×10 ⁻⁴	6840.7	1.0×10 ⁻⁵	14793.0	0.0
2MASS J01-24 b ^(c)	33.83 ^{+0.02} _{-0.06}	51.87 ^{+4.29} _{-3.97}	24.513 ^{+1.644} _{-1.644}	0.99 ^{+0.13} _{-0.13}	1947.3	1.3×10 ⁻⁴	6311.2	1.0×10 ⁻⁵	14060.1	0.0
2MASS J04+23 b ^(d)	145.00 ^{+0.00} _{-0.00}	15.00 ^{+0.00} _{-0.00}	7.334 ^{+1.808} _{-1.594}	3.61 ^{+1.20} _{-1.36}	1801.5	1.5×10 ⁻⁴	6065.7	1.0×10 ⁻⁵	13210.6	0.0
kap And b	50.06 ^{+0.56} _{-0.60}	55.04 ^{+1.30} _{-1.43}	24.513 ^{+8.812} _{-8.307}	1.25 ^{+0.10} _{-0.10}	1578.4	2.0×10 ⁻⁴	5436.9	2.0×10 ⁻⁵	12108.1	0.0
ROXs 42 B b	143.60 ^{+1.07} _{-1.11}	157.00 ^{+0.00} _{-0.00}	8.914 ^{+2.077} _{-2.077}	2.49 ^{+0.15} _{-0.15}	1211.7	3.3×10 ⁻⁴	4502.8	2.0×10 ⁻⁵	10016.2	0.0
PDS 70 b	113.08 ^{+0.33} _{-0.37}	20.06 ^{+1.31} _{-1.33}	2.967 ^{+0.686} _{-0.663}	2.88 ^{+0.22} _{-0.23}	1165.8	3.6×10 ⁻⁴	4119.2	3.0×10 ⁻⁵	8757.6	1.0×10 ⁻⁵
HIP 78530 b	136.70 ^{+1.03} _{-0.93}	741.60 ^{+39.77} _{-42.31}	22.987 ^{+0.647} _{-0.659}	1.84 ^{+0.10} _{-0.10}	1128.7	3.8×10 ⁻⁴	4401.6	3.0×10 ⁻⁵	10226.1	0.0
HR 8799 c	41.24 ^{+0.11} _{-0.10}	38.00 ^{+0.00} _{-0.00}	9.952 ^{+2.058} _{-1.965}	1.00 ^{+0.14} _{-0.14}	1003.7	4.9×10 ⁻⁴	3347.7	4.0×10 ⁻⁵	6721.2	1.0×10 ⁻⁵
COCONUTS-2 b	10.89 ^{+0.00} _{-0.00}	9106.99 ^{+2375.80} _{-2510.44}	6.067 ^{+1.142} _{-1.149}	1.11 ^{+0.02} _{-0.02}	980.4	5.1×10 ⁻⁴	2797.0	6.0×10 ⁻⁵	5843.0	1.0×10 ⁻⁵
HR 8799 d	41.24 ^{+0.11} _{-0.11}	24.00 ^{+0.00} _{-0.00}	10.151 ^{+1.998} _{-2.196}	0.89 ^{+0.14} _{-0.13}	978.0	5.1×10 ⁻⁴	3233.4	5.0×10 ⁻⁵	6504.8	1.0×10 ⁻⁵
HD 106906 b	102.99 ^{+0.35} _{-0.29}	650.00 ^{+0.00} _{-0.00}	11.025 ^{+1.315} _{-1.421}	1.60 ^{+0.00} _{-0.00}	950.6	5.4×10 ⁻⁴	3549.0	4.0×10 ⁻⁵	7802.0	1.0×10 ⁻⁵
HR 8799 e	41.25 ^{+0.10} _{-0.00}	16.98 ^{+0.98} _{-1.01}	11.477 ^{+3.894} _{-3.977}	0.90 ^{+0.14} _{-0.14}	947.0	5.5×10 ⁻⁴	3310.0	4.0×10 ⁻⁵	6679.0	1.0×10 ⁻⁵
WISEP J12+16 b ^(e)	10.10 ^{+0.00} _{-0.00}	8.07 ^{+0.81} _{-0.92}	21.917 ^{+1.948} _{-1.292}	0.87 ^{+0.13} _{-0.13}	920.1	5.8×10 ⁻⁴	2743.1	7.0×10 ⁻⁵	5735.7	1.0×10 ⁻⁵
GU Psc b	47.55 ^{+0.11} _{-0.11}	1999.45 ^{+135.25} _{-126.82}	11.368 ^{+1.131} _{-1.178}	1.18 ^{+0.02} _{-0.02}	871.6	6.4×10 ⁻⁴	3124.1	5.0×10 ⁻⁵	6630.2	1.0×10 ⁻⁵
PDS 70 c	113.06 ^{+0.34} _{-0.34}	35.42 ^{+3.26} _{-3.19}	1.998 ^{+0.702} _{-0.697}	2.44 ^{+0.40} _{-0.40}	856.5	6.7×10 ⁻⁴	3025.0	5.0×10 ⁻⁵	6415.4	1.0×10 ⁻⁵
CFHTWIR-Oph 98 b	137.00 ^{+0.00} _{-0.00}	199.91 ^{+4.19} _{-4.18}	7.732 ^{+0.341} _{-0.341}	1.86 ^{+0.03} _{-0.03}	832.8	7.1×10 ⁻⁴	3160.4	5.0×10 ⁻⁵	6978.2	1.0×10 ⁻⁵
HR 2562 b	34.01 ^{+0.03} _{-0.03}	20.30 ^{+0.20} _{-0.20}	29.554 ^{+10.914} _{-10.051}	0.56 ^{+0.01} _{-0.01}	739.4	9.0×10 ⁻⁴	2471.8	8.0×10 ⁻⁵	5066.1	2.0×10 ⁻⁵
1RXS J16-21 b ^(f)	139.15 ^{+0.91} _{-0.89}	330.00 ^{+0.00} _{-0.00}	7.973 ^{+0.665} _{-0.645}	1.70 ^{+0.00} _{-0.00}	697.4	1.0×10 ⁻³	2740.0	7.0×10 ⁻⁵	6291.5	1.0×10 ⁻⁵
HIP 65426 b	108.90 ^{+0.49} _{-0.53}	92.00 ^{+0.00} _{-0.00}	9.220 ^{+1.905} _{-1.926}	1.50 ^{+0.02} _{-0.02}	679.3	1.1×10 ⁻³	2616.7	7.0×10 ⁻⁵	5730.7	1.0×10 ⁻⁵
2MASS J12-39 b ^(g)	64.32 ^{+0.45} _{-0.45}	55.00 ^{+0.00} _{-0.00}	4.878 ^{+1.476} _{-1.333}	1.00 ^{+0.07} _{-0.21}	627.9	1.2×10 ⁻³	2529.6	8.0×10 ⁻⁵	5553.6	2.0×10 ⁻⁵
GJ 504 b	17.53 ^{+0.05} _{-0.05}	43.50 ^{+0.00} _{-0.00}	5.561 ^{+1.987} _{-1.786}	0.96 ^{+0.05} _{-0.05}	598.6	1.4×10 ⁻³	1635.3	1.8×10 ⁻⁴	3314.7	4.0×10 ⁻⁵
TYC 8998-760-1 c	94.63 ^{+0.18} _{-0.20}	320.00 ^{+0.00} _{-0.00}	6.007 ^{+0.679} _{-0.672}	1.25 ^{+0.31} _{-0.31}	489.2	2.1×10 ⁻³	1998.6	1.2×10 ⁻⁴	4297.1	3.0×10 ⁻⁵
HR 8799 b	41.25 ^{+0.10} _{-0.10}	68.00 ^{+0.00} _{-0.00}	7.952 ^{+2.050} _{-2.053}	0.60 ^{+0.07} _{-0.07}	469.9	2.2×10 ⁻³	1624.9	1.9×10 ⁻⁴	3293.2	5.0×10 ⁻⁵
51 Eri b	29.76 ^{+0.08} _{-0.08}	13.20 ^{+0.14} _{-0.14}	2.000 ^{+0.000} _{-0.000}	0.68 ^{+0.09} _{-0.10}	256.7	7.4×10 ⁻³	767.9	8.3×10 ⁻⁴	1493.2	2.2×10 ⁻⁴
HD 95086 b	86.23 ^{+0.15} _{-0.16}	55.77 ^{+1.68} _{-1.72}	4.987 ^{+1.368} _{-1.368}	0.85 ^{+0.07} _{-0.07}	220.8	1.0×10 ⁻²	915.9	5.8×10 ⁻⁴	1858.5	1.4×10 ⁻⁴
GQ Lup b	151.17 ^{+0.74} _{-0.72}	100.00 ^{+0.00} _{-0.00}	20.000 ^{+0.000} _{-0.000}	0.68 ^{+0.15} _{-0.14}	143.4	2.4×10 ⁻²	838.0	7.0×10 ⁻⁴	1853.4	1.4×10 ⁻⁴

Notes. The values given here are the result of our statistical methodology to simulate the planetary orbits (Sect. 2.1). Planets for which the quoted parameter uncertainties are 0.00 generally lack a value for the uncertainties in the NASA Archive.

^(a)2MASS J02192210-3925225 b ^(b)2MASS J21402931+1625183 A b ^(c)2MASS J01225093-2439505 b ^(d)2MASS J04414489+2301513 b ^(e)WISEP J121756.91+162640.2 A b ^(f)1RXS J160929.1-210524 b ^(g)2MASS J12073346-3932539 b

We compiled the list of young planets that have been already directly imaged from ground-based or space-borne observatories. We used the NASA Exoplanet Archive as reference and added the values of effective temperatures and radii from the literature. Table F.1 shows the LIFE integration times for these planets. In all cases we assumed 3 exozodis, although we note that some of these systems will have higher exozodi levels. We did not compute the observability with HWO since most of these young planetary systems were discovered using direct imaging techniques in the near-infrared (J, H, K-bands). Virtually all of these planets should also be detectable with future reflected-light missions in the visible (unless the OWA becomes a limitation), given that they will achieve much deeper contrasts compared to ground-based facilities.

The vast majority of these directly-imaged planets will already have their mid-IR spectra being measured with *JWST* or the ground-based ELTs and will not be prime targets for LIFE. However, constraining the required integration times with LIFE enables an interesting comparison between the different facilities. We note that *JWST* has roughly the same collecting power as the optimistic scenario of LIFE with four 3.5 m mirrors.